AD-A087 402 MCDONNELL DOUGLAS RESEARCH LABS ST LOUIS MO F/G 20/14
RADIATION AND SCATTERING FROM BODIES OF TRANSLATION. VOLUME I.(U)
APR 80 L N MEDGYESI-MITSCHANG F30602-77-C-0233
UNCLASSIFIED RADC-TR-80-142-VOL-1 NL

END
DATE
FILMED
9 80
DTIC

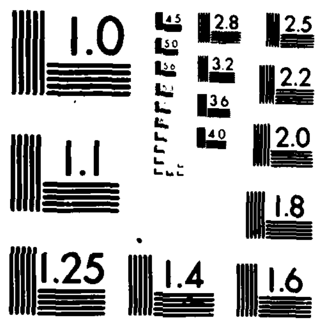

MICROCOPY RESOLUTION TEST CHART
NATIONAL BUREAU OF STANDARDS 1963-A

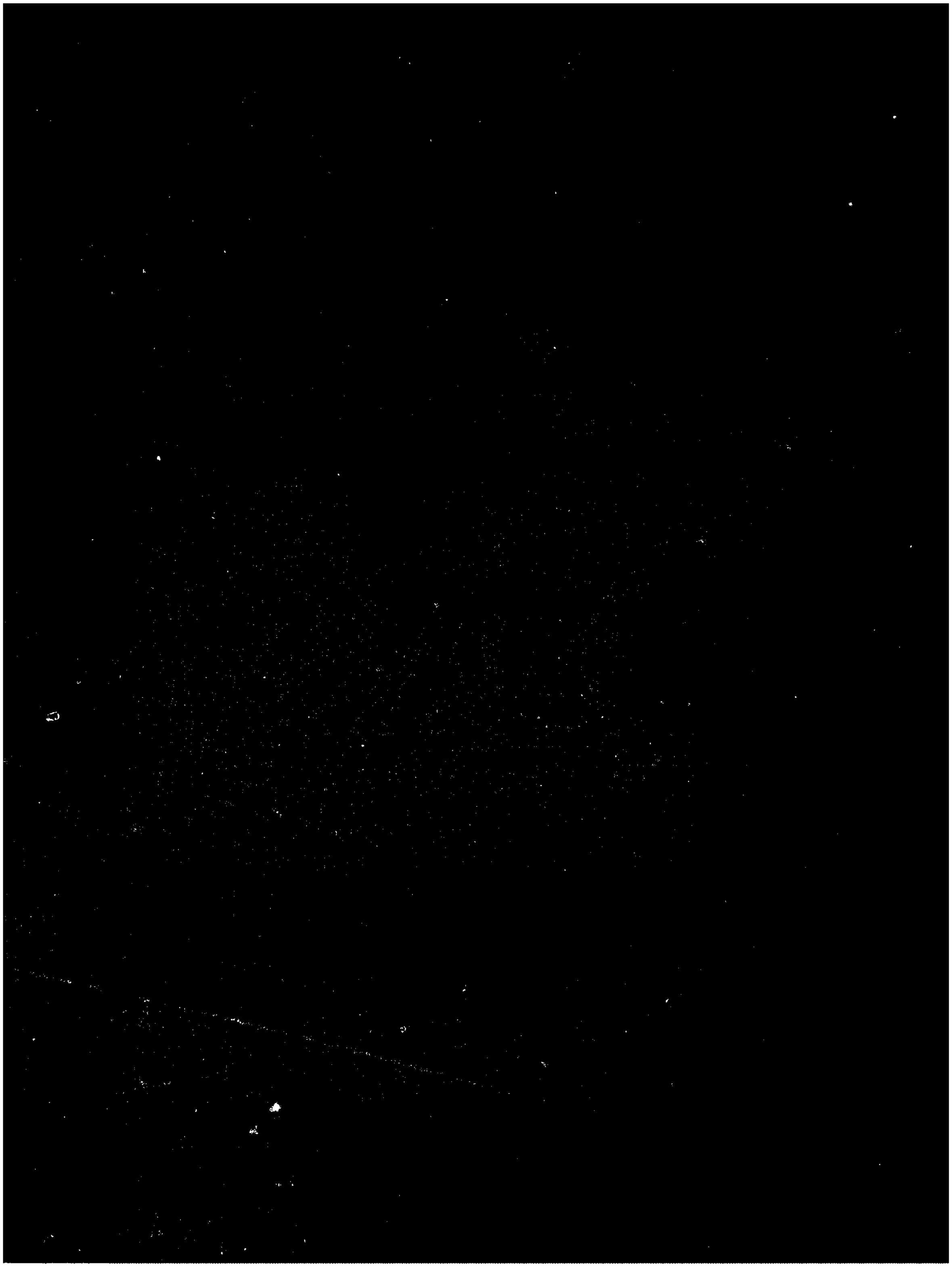

(19) TR-80-142-Vol-1

UNCLASSIFIED

SECURITY CLASSIFICATION OF THIS PAGE (When Data Entered)

REPORT DOCUMENTATION PAGE		READ INSTRUCTIONS BEFORE COMPLETING FORM
1. REPORT NUMBER (18) RADC-TR-80-142, Vol I (of three)	2. GOVT ACCESSION NO. AD-A087 402	3. RECIPIENT'S CATALOG NUMBER
4. TITLE (and Subtitle) (6) RADIATION AND SCATTERING FROM BODIES OF TRANSLATION. Volume I.		5. TYPE OF REPORT & PERIOD COVERED (9) Final Technical Report, 26 Sep 77 — 26 Jul 79
		6. PERFORMING ORG. REPORT NUMBER N/A
7. AUTHOR(s) (10) L. N. Medgyesi-Mitschang		8. CONTRACT OR GRANT NUMBER(s) (15) F30602-77-C-0233
9. PERFORMING ORGANIZATION NAME AND ADDRESS McDonnell Douglas Corporation McDonnell Douglas Research Laboratories St. Louis MO 63166		10. PROGRAM ELEMENT, PROJECT, TASK AREA & WORK UNIT NUMBERS 62702F (16) 2338 (17) 0308 03
11. CONTROLLING OFFICE NAME AND ADDRESS Rome Air Development Center (RBCT) Griffiss AFB NY 13441		12. REPORT DATE (11) Apr 1980
		13. NUMBER OF PAGES 67
14. MONITORING AGENCY NAME & ADDRESS(if different from Controlling Office) Same (12) 66		15. SECURITY CLASS. (of this report) UNCLASSIFIED
		15a. DECLASSIFICATION/DOWNGRADING SCHEDULE N/A

16. DISTRIBUTION STATEMENT (of this Report)

Approved for public release; distribution unlimited.

17. DISTRIBUTION STATEMENT (of the abstract entered in Block 20, if different from Report)

Same

18. SUPPLEMENTARY NOTES

RADC Project Engineer: Daniel E. Warren (RBCT)

19. KEY WORDS (Continue on reverse side if necessary and identify by block number)

Radiation	Method of moments
Scattering	Near field analysis
Conducting surfaces	Aperture coupling

20. ABSTRACT (Continue on reverse side if necessary and identify by block number)

An analytical formulation, based on the method of moments (MM) is described for solving electromagnetic problems associated with finite-length cylinders of arbitrary cross seciton, denoted in this report as bodies of translation (BOT). This class of bodies can be used to model structures with noncircular cross sections such as wings, fins, and aircraft fuselages. The theoretical development parallels in part the MM formulation developed earlier by Mautz and Harrington for bodies of

(Cont'd)

DD FORM 1 JAN 73 1473 EDITION OF 1 NOV 65 IS OBSOLETE

UNCLASSIFIED

SECURITY CLASSIFICATION OF THIS PAGE (When Data Entered)

405315

Item 20 (Cont'd)

revolution (BOR). Like the latter approach, a modal expansion is used to describe the unknown surface currents on the BOT. The present analysis has been developed to treat the far-field radiation and scattering from a BOT excited by active antennas or illuminated by a plane wave of arbitrary polarization and angle of incidence. In addition, the electric and magnetic near-field components are determined in the vicinity of active and passive apertures (slots). Using the Schelkunoff equivalence theorem, the aperture-coupled fields within a BOT are also obtained. The formulation has been implemented by a computer algorithm and validated using accepted data in the literature. A user/systems manual (Volume II) provides a detailed description of the use of the codes and example problems. Program listings are given in Volume III.

TABLE OF CONTENTS

LIST OF ILLUSTRATIONS

LIST OF ILLUSTRATIONS

EVALUATION

This report documents an electromagnetic (EM) fields analysis technique that was developed for a class of bodies that can be modeled as rectangular cylinders with an arbitrary cross sectional geometry, and are referred to as "Bodies of Translation" (BOT). This technique has the ability to model EM scattering, radiation with multiple antennas, aperture coupling, near and far electric and magnetic fields as well as surface current distribution.

This technique is presently limited to modeling BOT's which have open ends and slot antennas. A subsequent effort will address these limitations and develop procedures for modeling the ends of the BOT's and off-surface radiations such as monopoles and loops. Emphasis will also be placed on techniques which will allow one to hybrid this method with other EM analysis techniques in order to model the behavior of more complex structures as well as to economize computer resources.

Daniel E. Warren

DANIEL E. WARREN
Project Engineer

1. INTRODUCTION AND BACKGROUND

Modern aircraft and missiles require complex electromagnetic (EM) systems to perform their roles effectively. To characterize the behavior of these systems, analytical techniques have been developed to predict the EM radiation generated and scattered by aerospace vehicles. Recently, predictive techniques based on the method of moments (MM) have been developed to solve a variety of antenna, coupling, and field penetration problems.[1] In these analyses, the radiating or scattering structures are represented by wires, surface patches, and wire grids. Because of the computational requirements of the method to date, application of these methods has been limited to bodies with surface areas on the order of λ^2. Larger surfaces (of $\sim 45\ \lambda^2$) can be analyzed via the MM technique if the vehicle body has some degree of symmetry, such as in the case of bodies of revolution (BOR).

To treat complex-shaped bodies, such as parts of wing sections and noncircular aircraft fuselages, a generalized theoretical formulation called the method of moments for bodies of translation, abbreviated here as MM/BOT, has been developed.[2,3] This formulation treats the radiation and scattering from bodies with active and passive apertures. In addition, the technique has been extended to compute the fields in the immediate vicinity of a slot antenna as well as fields coupled interiorly through rectangular apertures in the BOT surface. The MM/BOT technique combines many of the cost-effective features of the MM/BOR analysis[4] with some of the shape flexibility of the wire-grid approach and retains the ability to treat difficult boundary conditions associated with realistic radiating and scattering geometries.

2. SUMMARY OF COMPLETED EFFORT

The principal results of the completed effort are enumerated below. Detailed discussion of the individual topics is given in the sections indicated.

- The MM/BOT formulation was developed for a generalized BOT configuration to treat the radiation from asymmetric aperture (slot) antennas or arrays (Sections 4 and 5). The results are in agreement with the predictions of the MM/BOR technique for asymmetric slots embedded in a BOR surface (Section 8).
- The MM/BOT formulation was extended to compute all the electric and magnetic near-field components at an arbitrary point in the vicinity of a radiating or scattering surface. For radiating apertures, an arbitrary polarization and antenna excitation can be specified (Section 6).
- An analysis was implemented to determine the aperture-coupled fields (both electric and magnetic) produced by EM illumination of the BOT from an arbitrary angle of incidence and polarization (Section 7).
- A computer algorithm was developed to implement all aspects of the MM/BOT formulation in a hierarchy of user-oriented computer codes. The codes, written in FORTRAN IV, are modular and machine independent. All parts of the codes were tested and installed on the RADC computer system. A user/systems manual (Volume II of this report) was developed for the MM/BOT algorithm. A series of example problems was provided to illustrate the technique for the prospective user.
- The entire computer algorithm was tested for a series of EM problems and validated with results using classical boundary value solutions and the MM/BOR codes (Section 8).

3. SUMMARY OF PREVIOUS WORK

The original formulation of the method of moments (MM) was applied initially to treat the radiation and scattering from thin wire structures[1,5] and later to bodies of revolution.[4] As shown in the subsequent discussion, the MM theory can be extended to treat finite cylindrical bodies of arbitrary cross section, denoted here as bodies of translation (BOT). Examples of such configurations are shown in Figure 1. In this report, the cylinders are assumed to be uncapped (i.e., open at the ends). The theoretical development for this class of bodies parallels in part the MM/BOR formulation[4] and retains the modal expansion concept developed in the latter theory.

Earlier, Andreasen[6], Wallenberg and Harrington[7], and Wilton and Mittra[8], among others, have treated the case of cylinders of arbitrary cross section but of infinite length. The case of finite-length cylinders of arbitrary cross sections has not been treated previously. Several investigators examined the special case of finite-length, right-circular cylinders for various limiting cases. For example, Ufimtsev[9], Kieburtz[10], and Fialkovskii[11] developed solutions for thin cylinders with $ka \ll 1$; while Adey[12] considered long cylinders with $ka = 1$, where $ka = 2\pi a/\lambda$ and a is the cylinder radius. Williams[13] studied the diffraction from finite-length hollow cylinders where the open ends did not materially influence the diffracted waves. A complete study of tubular cylinders was made by Kao[14,15] for arbitrary length and ka, but restricted to broadside illumination. His formulation resulted in a pair of decoupled integral equations that were solved to yield the axial and the circumferential currents on the cylinder. Recently, Davis and Mittra[16] examined the current distribution on an open cylinder of 1 λ length and $ka = 1$ using a hybrid formulation incorporating the electric and magnetic field integral equation representations of Maxwell's equations (i.e., EFIE and MFIE, respectively). The present MM/BOT formulation treats the foregoing problems as special subcases.

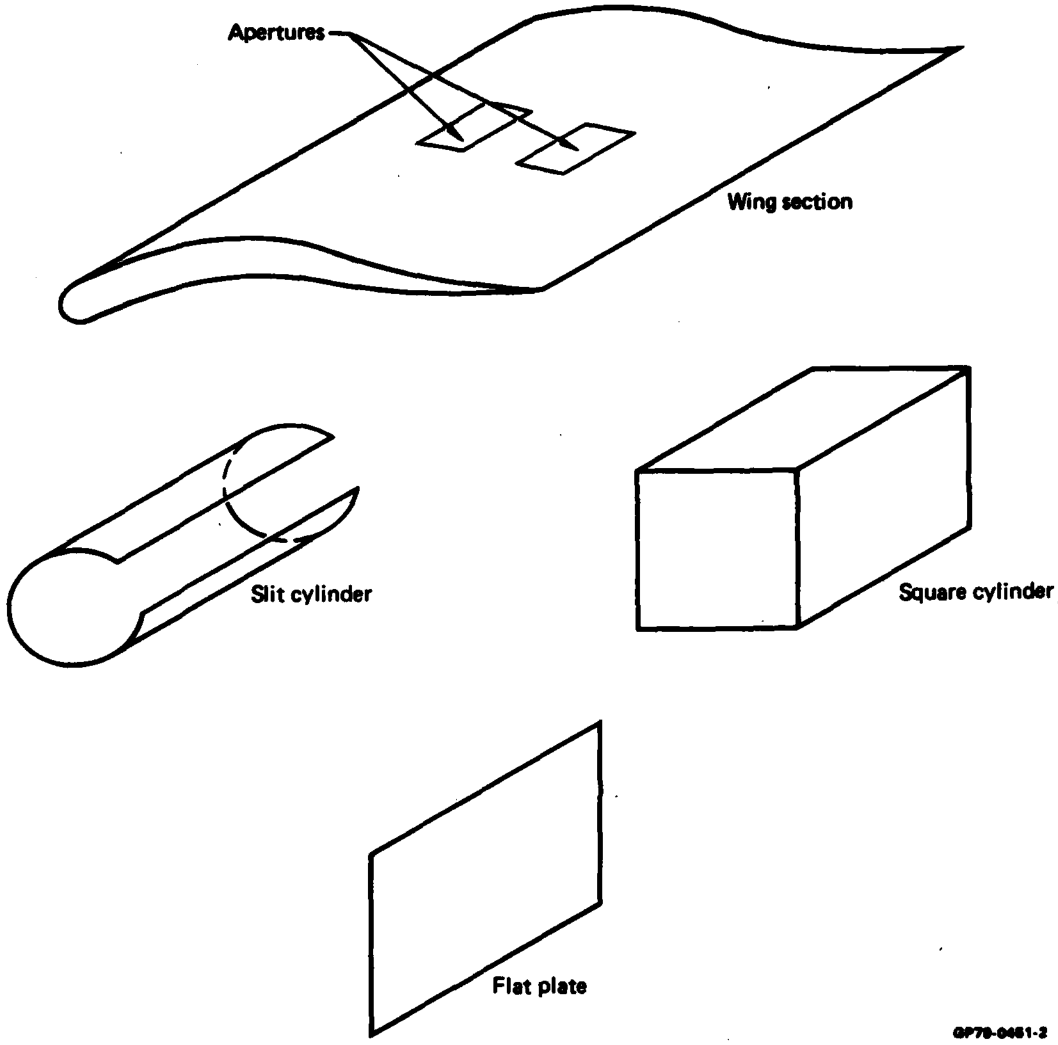

Figure 1. Body of translation (BOT) configurations.

4. DEVELOPMENT OF MM/BOT FORMULATION

4.1 Electric Field Integral Equation for BOT

In a given radiation or scattering problem, the total electric field is given as

$$\vec{E} = \vec{E}^i + \vec{E}^s, \tag{1}$$

where i and s refer to the incident and scattered fields, respectively. The scattered field in turn is defined in terms of the vector potential, $\vec{A}$, and scalar potential, Φ, yielding

$$\vec{E}^s = -j\omega\vec{A} - \nabla\Phi, \tag{2}$$

$$\vec{A} = \mu_o \iint_S \vec{J} \frac{e^{-jkR}}{4\pi R} ds, \tag{3}$$

$$\Phi = \frac{1}{\varepsilon_o} \iint_S \sigma \frac{e^{-jkR}}{4\pi R} ds, \tag{4}$$

$$\sigma = \frac{j}{\omega} \nabla \cdot \vec{J}. \tag{5}$$

The field at the surface of the conductor can be expressed in terms of the incident and scattered electric fields E^i and E^s, respectively, i.e.,

$$\vec{E}^s_{tan} = -\vec{E}^i_{tan} = -[j\omega\vec{A}(\vec{J}) + \nabla\Phi(\vec{J})]_{tan} \equiv L(\vec{J}), \tag{6}$$

where $\vec{J}$ is the unknown current density on the surface and $L(\cdot)$ is a linear integro-differential operator over $\vec{J}$. Writing out Equation (6) explicitly yields

$$\vec{E}^i_{tan} = j\omega\mu_o \left[\iint_S \vec{J} \frac{e^{-jkR}}{4\pi R} ds + \frac{1}{\omega^2\mu_o\varepsilon_o} \nabla' \iint_S (\nabla\cdot\vec{J}) \frac{e^{-jkR}}{4\pi R} ds \right]_{tan} \equiv \vec{L}(\vec{J}). \tag{7}$$

4.2 Expansion of Surface Currents

Restricting the discussion to a BOT, Equation (7) is solved for $\vec{J}$ by subdividing the domain of the integro-differential equation by segmenting the BOT surface S into length-wise strips as shown in Figure 2. On the conducting surface S of the scatterer (Figure 2), the unknown current density $\vec{J}$ is expanded in a double sum of basis functions spanning S, described by the orthonormal coordinates (t,z), so that

$$\vec{J} = \vec{J}^t + \vec{J}^z = \sum_{j,n} \left\{ \vec{u}_t I^t_{nj} f^t_j(\tau) + \vec{u}_z I^z_{nj} f^z_j(\tau) \right\} v_n(\zeta), \quad (8)$$

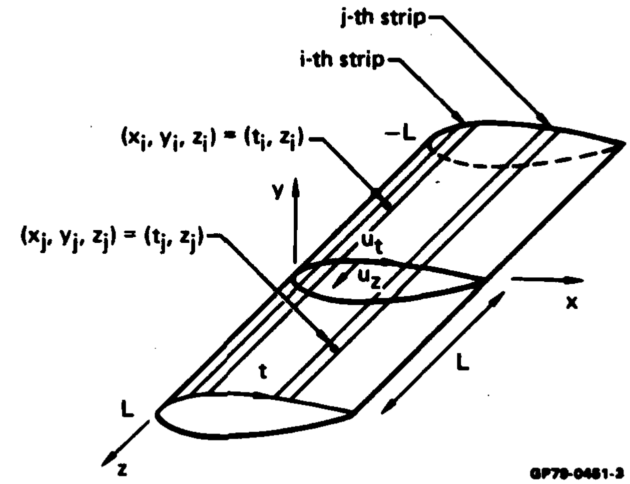

Figure 2. Segmented BOT configuration.

where $\zeta = z/L$, $\tau = t/\Gamma$, and $v_n(\zeta)$ is to be defined later. (L is the half-length of the scattering body along z, and Γ is the girth of S along t divided by the number of strips chosen to represent S.) Equation (8) implies a modal expansion of J along ζ. The terms $f^t_j(\tau)$ and $f^z_j(\tau)$ can be chosen as pulse, piecewise sinusoidal, or, as in this case, triangle functions, i.e.,

$$f^\alpha_j(\tau) = \begin{cases} 1 - |\tau'|, |\tau'| < 1 \\ 0, |\tau'| > 1 \end{cases}, \ \tau' = \tau - \tau_j, \ \alpha = t \text{ or } z. \quad (9)$$

For a nonclosed BOT (i.e., the slit cylinder in Figure 1), a half-triangle function is used to expand the currents along an edge parallel to z. The choice of triangle functions allows compact, computer-coefficient expressions to be obtained for the MM impedance expressions. Substituting Equation (8) into Equation (7) and forming the inner products via the Galerkin procedure with respect to a set of trial functions $\vec{W}^{\alpha}_{ni}(=\vec{J}^{\alpha}_{ni})$, with α = t or z, yields the matrix equation,

$$\begin{bmatrix} V_{-n} \\ \cdot \\ \cdot \\ V_o \\ \cdot \\ \cdot \\ V_n \end{bmatrix} = \begin{bmatrix} & & \\ & Z_{BOT} & \\ & & \end{bmatrix} \begin{bmatrix} I_{-n} \\ \cdot \\ \cdot \\ I_o \\ \cdot \\ \cdot \\ I_n \end{bmatrix} . \tag{10}$$

In Equation (10), the column vectors V and I refer to the equivalent voltages and currents on S, respectively, and where the i-th element of V in terms of the inner product for the n-th mode is defined as:

$$\begin{aligned} V^{\alpha}_{ni} &= \frac{1}{\Gamma L} \left\langle \vec{E}^{i}_{tan}, \vec{W}^{\alpha}_{ni} \right\rangle \\ &= \int_S ds\ \vec{E}^{i}_{tan} \cdot \vec{W}^{\alpha}_{ni} = \int_S ds\ \vec{E}^{i}_{tan} \cdot \vec{u}_{\alpha}\ f^{\alpha}_{i}(\tau)\ v_n(\zeta), \end{aligned} \tag{11}$$

where V^{α}_{ni}, with α = t or z, denotes the α-directed voltage on the BOT.

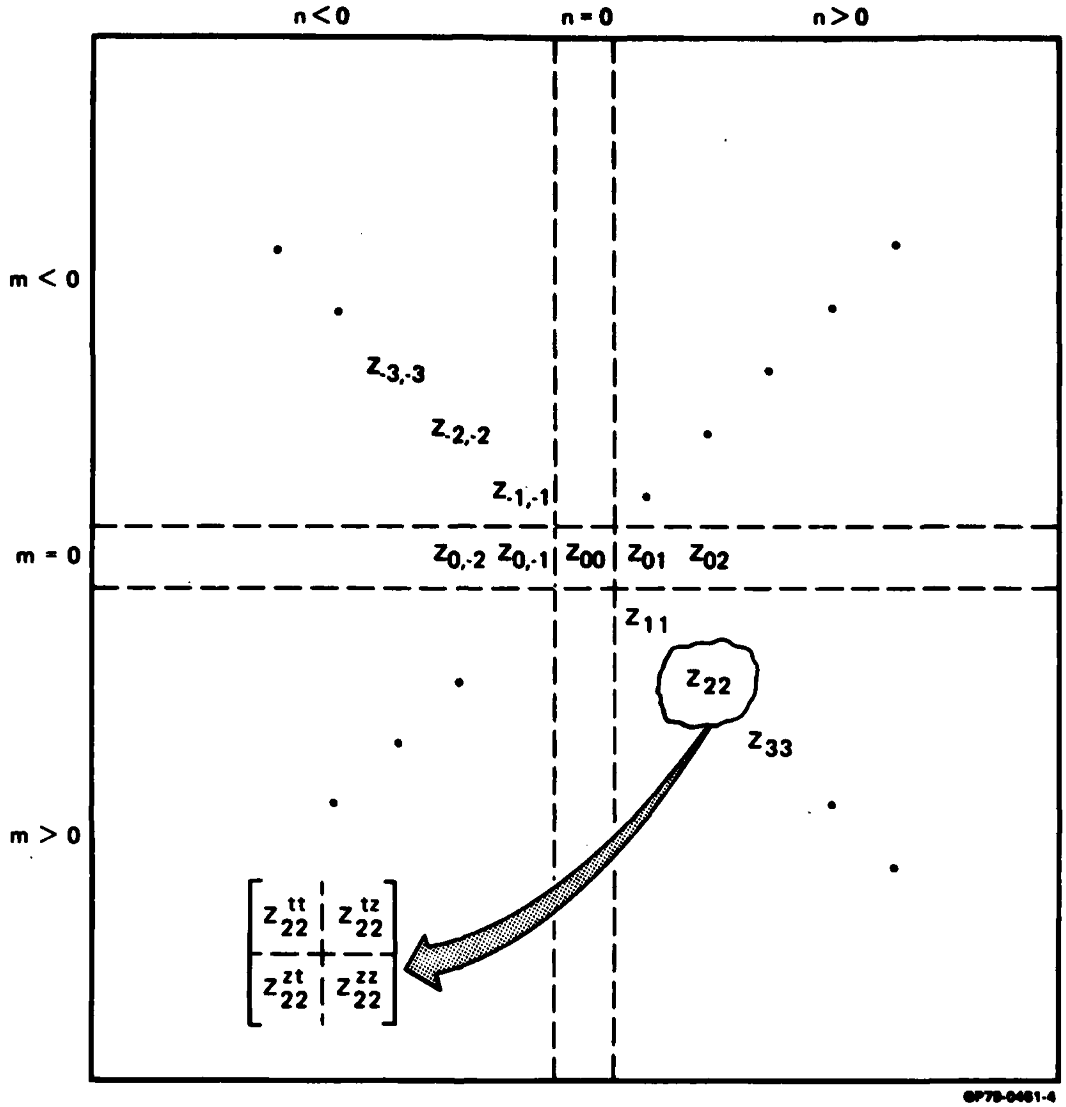

Figure 3. General structure of impedance matrix for MM/BOT analysis.

4.3 Derivation of the Impedance Matrix, Z_{BOT}

The structure of Z_{BOT} is given in Figure 3, where each Z_{mn} is a full submatrix. The foregoing matrix equation bears a canonic similarity to the MM/BOR result. However, in general, the expansion functions in Equation (8) are not orthonormal with respect to the integral operator $L(\cdot)$ over the surface of the BOT as in the BOR case. Thus, in principle, all the Z_{mn} matrices are present in Z_{BOT}, since there is no modal decoupling. The elements of the partitioned submatrices of Z_{mn} can be computed from the general expression:

$$\left(Z^{\alpha\beta}_{ij}\right)_{mn} = \iint_S ds \iint_{S'} ds' \left[j\omega\mu_o \, \vec{W}^{\alpha}_{mi}(s') \cdot \vec{J}^{\beta}_{nj}(s) + \frac{1}{j\omega\epsilon_o} \left(\nabla' \cdot \vec{W}^{\alpha}_{mi}(s')\right)\left(\nabla \cdot \vec{J}^{\beta}_{ni}(s)\right)\right] \cdot \frac{e^{-jkR}}{4\pi R} , \tag{12}$$

where

$$(\alpha, \ \beta = t \text{ or } z) \text{ and } R = \sqrt{(x - x')^2 + (y - y')^2 + (z - z')^2} .$$

Using the expansion for $\vec{J}$ [Equation (8)] and the fact that $\vec{W}_{ni} = \vec{J}^{*}_{ni}$ (* denotes a conjugate) and noting that for any vector $\vec{A}$, $\nabla \cdot \vec{A} = \Gamma^{-1} \partial A_t / \partial\tau) + L^{-1}(\partial A_z / \partial\zeta)$, Equation (8) becomes:

$$\left(Z^{tt}_{ij}\right)_{mn} = jK\eta\delta \int_S ds \int_{S'} ds' \left(\cos(\nu - \nu') \, f^t_i(\tau) \, f^t_j(\tau') - \frac{1}{\delta^2 K} \, \dot{f}^t_i(\tau') \, \dot{f}^t_j(\tau) \right) v^*_m(\zeta') \, v_n(\zeta) \, \Phi, \tag{13}$$

$$\left(Z^{tz}_{ij}\right)_{mn} = \frac{\eta}{jK} \int_S ds \int_{S'} ds' \, \dot{f}^t_i(\tau') \, f^z_j(\tau) \, v^*_m(\zeta') \, \dot{v}_n(\zeta) \, \Phi, \tag{14}$$

and

$$\left(Z_{ij}^{zz}\right)_{mn} = jK\eta\delta \int_S ds \int_{S'} ds' \left(v_m^*(\zeta')v_n(\zeta) - \frac{1}{K^2} \dot{v}_m^*(\zeta')\dot{v}_n(\zeta)\right) \cdot f_i^z(\tau)\ f_j^z(\tau')\ \Phi \tag{15}$$

where

$$ds = d\tau d\zeta;\ \eta = \sqrt{\frac{\mu_o}{\varepsilon_o}}\ ;\ \delta = \frac{\Gamma}{L}\ ;\ K = 2\pi\left(\frac{L}{\lambda}\right)$$

and

$$\Phi = \frac{1}{4\pi} \frac{e^{-jK\sqrt{\delta^2\rho^2 + (\zeta - \zeta')^2}}}{\sqrt{\delta^2\rho^2 + (\zeta - \zeta')^2}}$$

$$\rho = \frac{1}{\Gamma}\sqrt{(x - x')^2 + (y - y')^2}\ , \tag{16}$$

and ν and ν' are the angles between the t-curve and the x-axis at points x,y and x',y' on the BOT, respectively. The expression for $(Z_{ij}^{zt})_{mn}$ is identical to that given in Equation (14), with m and n, and i and j interchanged. For evaluation of Equations (13-15), the functional form of $v_n(\zeta) = \exp(jn\pi\zeta)$ was chosen. The triangle function $f_j(\cdot)$, [Equation (9)], and its derivative $\dot{f}_j(\cdot)$ are approximated by four pulses, denoted as T_p and $\dot{T}_p$, respectively, with p = 1, 2, 3, 4 where

$$T_p = \left\{\frac{1}{8}, \frac{3}{8}, \frac{3}{8}, \frac{1}{8}\right\} \text{ and } \dot{T}_p = \left\{\frac{1}{2}, \frac{1}{2}, -\frac{1}{2}, -\frac{1}{2}\right\}.$$

The expressions for the (i,j)-th elements of the submatrices of Z_{BOT} are obtained by carrying out the surface integrals in Equations (13-15). The corresponding triangle functions are depicted graphically in Figure 4. Thus,

$$\left(Z_{ij}^{tt}\right)_{mn} = j2K\eta\delta \sum_{p,q=1}^{4} \left[T_p^t T_q^t \cos(\nu_p - \nu_q) - \frac{1}{\delta^2 K^2} \dot{T}_p^t \dot{T}_q^t\right] G_{mn} \tag{17}$$

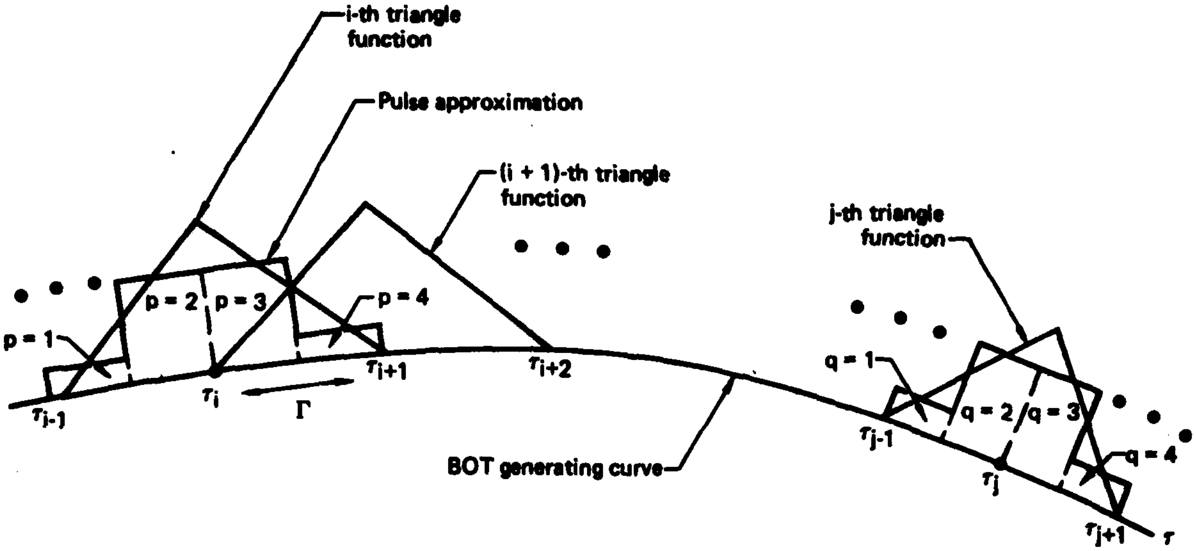

Figure 4. Pulse approximation for triangle functions on BOT surface.

$$\left(Z_{ij}^{tz}\right)_{mn} = \frac{2\pi n}{K}\,\eta \sum_{p,q=1}^{4} \dot{T}_p^t T_q^z \; G_{mn} \tag{18}$$

$$\left(Z_{ij}^{zt}\right)_{mn} = -\frac{2\pi m}{K}\,\eta \sum_{p,q=1}^{4} T_p^z \dot{T}_q^t \; G_{mn} \tag{19}$$

$$\left(Z_{ij}^{zz}\right)_{mn} = j2K\eta\delta \sum_{p,q=1}^{4} T_p^z T_q^z \left(1 - \frac{mn\pi^2}{K^2}\right) G_{mn} \; , \tag{20}$$

where following the convention in Reference 4, (i,j) correspond to the indexes p,q, respectively. The term ν_p is the angle between the t-curve and the x-axis at point x_p, y_p on the BOT. The function G_{mn} is the Green's function integrated over ds and ds', where these integrations can be carried out quasi-analytically, as discussed below.

4.4 Evaluation of G_{mn} Functions

The evaluation of G_{mn} encompasses two surface integrals, written explicitly as:

$$G_{mn}(i,j) = \int_p d\tau' \int_q d\tau \int_{-1}^{1} d\zeta \int_{-1}^{1} d\zeta' \frac{e^{-jK\sqrt{\delta^2 \rho^2 + (\zeta - \zeta')^2}}}{4\pi \sqrt{\delta^2 \rho^2 + (\zeta - \zeta')^2}} \tag{21}$$

$$\cdot \; e^{j\pi(n\zeta - m\zeta')},$$

where the τ' and τ integrations are carried out over the p and q-th subsegments (strips) associated with the i-th and j-th strips (see Figure 4). Letting $\xi = \zeta - \zeta'$, the two integrations over ζ and ζ' reduce to

$$G_{mn}(i,j) = \int_0^2 d\xi \; u_{mn}(\xi) \int_p d\tau' \int_q d\tau \; \frac{e^{-jKR}}{R} \tag{22}$$

where

$$u_{mn}(\xi) = \begin{cases} \frac{1}{\pi}\left(1 - \frac{\xi}{2}\right) \cos n\pi\xi; \; m = n \\ \frac{1}{\pi} \frac{(-1)^{m-n+1}}{(n-m)\pi} \sin \left(\frac{n-m}{2}\right) \pi\xi \; \cos\left(\frac{n+m}{2}\right)\pi\xi; \; m \neq n \end{cases} \tag{23}$$

and

$$R = \sqrt{\delta^2 \rho^2 + \xi^2} \quad \text{and} \quad \rho^2 = \frac{1}{\Gamma^2} \left[(x - x')^2 + (y - y')^2\right].$$

The integral over τ' using the centroid approximation over the interval $\Delta\tau_p'$ yields

$$G_{mn}(i,j) = \int_0^2 d\xi \; u_{mn}(\xi) \; (\Delta\tau_p') \int_{\tau_1}^{\tau_2} d\tau \; \frac{e^{-jKR_p}}{R_p}, \tag{24}$$

where

$$R_p = \sqrt{\delta^2 \rho_p{}^2 + \xi^2}\,, \quad \rho_p^2 = \frac{1}{\Gamma^2}\left[(x - x_p)^2 + (y - y_p)^2\right],$$

and

$$\tau_1 = j + \left(\frac{q - 3}{2}\right), \; \tau_2 = j + \left(\frac{q - 2}{2}\right).$$

The integration over τ can be carried out analytically using a Taylor expansion of the integrand about R_{pq} and completing the square in the integrand. Using only one term in this expansion yields

$$\int_{\tau_1}^{\tau_2} d\tau \, \frac{e^{-jKR_p}}{R_p} \simeq e^{-jKR_{pq}} \int_{\tau_1}^{\tau_2} d\tau$$

$$\cdot \left\{ \frac{1 - jK\left[\sqrt{\delta^2(\tau + \tau_0)^2 + d^2} - \sqrt{\delta^2 \rho_{pq}{}^2 + \xi^2}\right]}{\sqrt{\delta^2(\tau + \tau_0)^2 + d^2}} \right\} \tag{25}$$

$$= e^{-jKR_{pq}} \left\{ - jK(\tau_2 - \tau_1) + (1 + jKR_{pq}) \frac{1}{\delta} \int_{s_1}^{s_2} \frac{ds}{\sqrt{s^2 + d^2}} \right\},$$

where

$$s = \delta\tau, \; \tau_0 = \frac{1}{\Gamma} \left| \left[(x_q - x_p) \cos \nu_q + (y_q - y_p) \sin \nu_q\right] \right|,$$

$$\left.\begin{matrix}\tau_1 \\ \tau_2\end{matrix}\right\} = \tau_0 \mp \frac{1}{4} \quad \text{and} \quad R_{pq} = \sqrt{\delta^2 \rho_{pq}{}^2 + \xi^2}\,,$$

$$\rho_{pq}^2 = \frac{1}{\Gamma^2}\left[(x_q - x_p)^2 + (y_q - y_p)^2\right].$$

$$d^2 = R_{pq}^2 - \delta^2 \tau_o^2$$

The approximation in Equation (25) implies the condition that

$$K \left| R_p - R_{pq} \right| \leq \frac{\pi}{2} \left(\frac{\Gamma}{\lambda} \right).$$

The integration over s in Equation (25) is carried out analytically. Then approximating the integral over ξ in Equation (24) by a series,

$$G_{mn} = \frac{2}{M} \sum_{\mu=0}^{M-1} u_{mn}(\xi_u) f(\xi_\mu), \tag{26}$$

where

$$f(\xi_\mu) = \frac{1}{\delta} e^{-jKR_{pq}} \left(1 + jKR_{pq} \right) \ln \chi \tag{27}$$

$$\chi = \left[\frac{s_2 + \sqrt{s_2^2 + d^2}}{s_1 + \sqrt{s_1^2 + d^2}} \right] - j \frac{K}{2}; \tag{28}$$

and

$$\left. \begin{matrix} s_1 \\ s_2 \end{matrix} \right\} = \delta(\tau_o \mp 1/4), \quad \xi_\mu = \frac{2\mu + 1}{M}.$$

For the self-terms (i.e., $\rho_{pq} = 0$), Equation (24) reduces to the form,

$$G_{mn} = \frac{2}{\delta} \int_0^2 d\xi \; u_{mn}(\xi) e^{-jK\xi} \left\{ - jK \frac{\delta}{4} + (1 + jK\xi) \left[\ln \left(\frac{\delta}{4} + \sqrt{\frac{\delta^2}{16} + \xi^2} \right) - \ln\xi \right] \right\}.$$

The integral over ξ can be evaluated numerically via Gaussian quadrature or a Simpson integration routine after an integration by parts to soften the ln ξ singularity at the lower limit. Thus,

$$G_{mn} = \frac{2}{\delta}\int_0^2 d\xi\, e^{-jK\xi}\left\{ u_{mn}(\xi)\left[-jK\frac{\delta}{4} + (1 + jK\xi)\ln\left(\frac{\delta}{4} + \sqrt{\frac{\delta^2}{16} + \xi^2}\right)\right.\right.$$

$$\left.\left. - jK\xi\,(\ln\xi - 1) - jK\xi\ln\xi\right] - \xi u'_{mn}(\xi)\,(\ln\xi - 1)\right\}. \qquad (29)$$

This completes the evaluation of the elements of the Z_{BOT} matrix. The analytical and computational complexity involved in this analysis is approximately equivalent to that encountered in the MM/BOR formulation. Thus, the matrix fill times for each impedance element in MM/BOR and MM/BOT are about the same. Furthermore, detailed examination of the $G_{mn}(i,j)$ function shows that it is maximum when $m = n$ and $i = j$, i.e., the largest values occur on the main diagonal of the Z_{BOT} matrix, and the self-terms contribute the most. These properties lead to a diagonally strong overall matrix that is intercoupled significantly only for the neighboring modes. Computer simulations have confirmed this feature.

4.5 General Structure of the Impedance Matrix

Using the results obtained for the individual members of the partitioned submatrices in Equations (17-20), the overall impedance matrix for a BOT can be constructed as shown in Figure 3. In general, this matrix is full since there is no modal decoupling. (In the MM/BOR analysis, only the matrices Z_{mm} along the principal diagonal are present.) However, certain symmetries exist for the G_{mn} and Z_{mn} that reduce the fill time of the Z_{BOT} matrix. Specifically,

$$\begin{aligned} G_{mn} &= {}_t(G_{mn}) \\ Z^{tt}_{mn} &= {}_t(Z^{tt}_{mn}) \\ m_t(Z^{tz}_{mn}) &= -\,n(Z^{zt}_{mn}) \\ Z^{zz}_{mn} &= {}_t(Z^{zz}_{mn}), \end{aligned} \qquad (30)$$

where ${}_t(G_{mn})$ denotes the transpose of G_{mn}. In the implementation of the analysis, only the lower triangular quadrant of the Z_{BOT} matrix is computed, i.e., the partitioned submatrices are filled for $0 \leq m <$ NMODE, and $-m \leq n \leq m$, where NMODE is the total number of axial modes (including $m = 0$) used in this analysis. To compute the inverse of Z_{BOT}, the entire Z_{BOT} matrix must be filled, which can be accomplished from the following symmetry relationships:

$$
\begin{array}{lll}
\underline{(n,m)} & \underline{(-m,-n)} & \underline{(-n,-m)} \\
Z^{tt}_{n,m} = Z^{tt}_{m,n} & = Z^{tt}_{m,n} & = Z^{tt}_{m,n} \\
Z^{zt}_{n,m} = -\,{}_t\left(Z^{tz}_{m,n}\right) & = -\,Z^{zt}_{m,n} & = {}_t\left(Z^{tz}_{m,n}\right) \\
Z^{tz}_{n,m} = -\,{}_t\left(Z^{zt}_{m,n}\right) & = -\,Z^{tz}_{m,n} & = {}_t\left(Z^{zt}_{m,n}\right) \\
Z^{zz}_{n,m} = Z^{zz}_{m,n} & = Z^{zz}_{m,n} & = Z^{zz}_{m,n}\,.
\end{array}
\tag{31}
$$

These relations are exploited in the MM/BOT computer algorithm to minimize the fill-time and aid in the solution of the matrix equations arising in the formulation. If the BOT has several (physical) planes of symmetry, additional relationships can be established within each of the partitioned submatrices, again allowing savings to be made in the computational requirements. In summary, the MM/BOT formulation yields an overall network representation composed of diagonally strong matrices, possessing certain symmetries and appearing to be intercoupled significantly only for neighboring modes.

5. FAR-FIELD RADIATION AND SCATTERING ANALYSIS

Having obtained the expressions for the Z_{BOT} matrix, the currents on the body can be obtained by solving the network matrix equation for the current vector I. In turn, knowing I, the radiated or scattered fields can be obtained as in the MM/BOR analysis if the radiation transfer matrices $R_n^{t\theta}$, $R_n^{z\theta}$, $R_n^{t\phi}$, and $R_n^{z\phi}$ are given. Formally, the i-th element of the transfer matrices is defined as

$$(R_n^{\alpha u})_i = \left\langle \vec{J}_{ni}^{\alpha}, \vec{E}_r^u \right\rangle \tag{32}$$

where the superscript α denotes t or z, and u denotes the θ or ϕ polarization of the radiated field E_r^u. In spherical coordinates,

$$\vec{E}_r^u = \vec{u}_r^u \, e^{jk(\rho\sin\theta_r \cos\phi_r + z\cos\theta_r)}, \tag{33}$$

where the field point of measurement is at θ_r, ϕ_r, and ρ is the distance to a point on the BOT surface, measured from the origin (see Figure 5). Expressing the inner product in Equation (32) explicitly, the transfer matrices are given as:

$$(R_n^{t\theta})_i = \Gamma L \int_i d\tau \int_{-1}^{1} d\zeta (\vec{u}_t \cdot \vec{u}_\theta^r) \, f_i^t(\tau) \, v_n(\zeta) \, e^{jk\psi} \tag{34}$$

$$(R_n^{z\theta})_i = \Gamma L \int_i d\tau \int_{-1}^{1} d\zeta (\vec{u}_z \cdot \vec{u}_\theta^r) \, f_i^z(\tau) \, v_n(\zeta) \, e^{jk\psi} \tag{35}$$

$$(R_n^{t\phi})_i = \Gamma L \int_i d\tau \int_{-1}^{1} d\zeta (\vec{u}_t \cdot \vec{u}_\phi^r) \, f_i^t(\tau) \, v_n(\zeta) \, e^{jk\psi} \tag{36}$$

$$(R_n^{z\phi})_i = 0 \; . \tag{37}$$

$$\psi = \rho\sin\theta_r \cos\phi_r + z\cos\theta_r$$

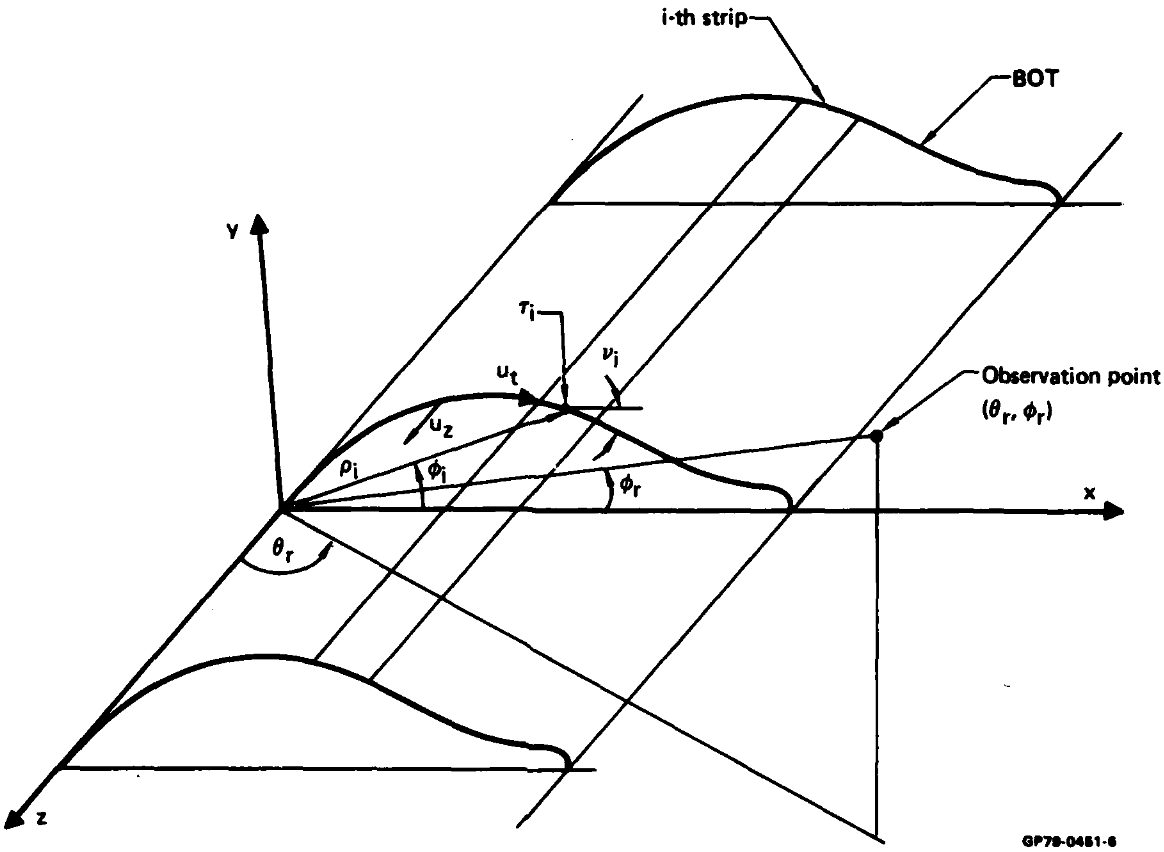

Figure 5. Coordinate geometry for transfer matrix evaluation.

Referring to Figure 5, the unit vectors for the BOT geometry are given by:

$$\vec{u}_t = \vec{u}_x \cos\nu + \vec{u}_y \sin\nu$$

$$\vec{u}_\phi = - \vec{u}_x \sin\phi + \vec{u}_y \cos\phi$$

and

$$\vec{u}^r_\theta = \vec{u}_x \cos\theta_r \cos\phi_r + \vec{u}_y \cos\theta_r \sin\phi_r - \vec{u}_z \sin\theta_r$$

$$\vec{u}^r_\phi = - \vec{u}_x \sin\phi_r + \vec{u}_y \cos\phi_r .$$

Using a centroid approximation for the t-integration, a pulse approximation for the triangle functions $f_i(\cdot)$ and letting $v_n(\zeta) = \exp(jn\pi\zeta)$ in Equations (34-36), the expressions for the i-th element of the transfer matrices become

$$(R_n^{t\theta})_i = \alpha \cos\theta_r \sum_{q=1}^{4} A_q^r T_q^t \cos(\nu_q - \phi_r) \tag{38}$$

$$(R_n^{z\theta})_i = -\alpha \sin\theta_r \sum_{q=1}^{4} A_q^r T_q^z \tag{39}$$

$$(R_n^{t\phi})_i = \alpha \sum_{q=1}^{4} A_q^r T_q^t \sin(\nu_q - \phi_r) \tag{40}$$

$$(R_n^{z\phi})_i = 0 , \tag{41}$$

where

$$A_q^r = e^{jk\rho_q \sin\theta_r \cos(\phi_q - \phi_r)}$$

$$\alpha = 2\,\Gamma L\, \mathrm{sinc}(\xi)$$

$$\xi = (n + \frac{2L}{\lambda}\cos\theta_r)\pi.$$

Using the R-matrices above, the far-field power radiation patterns and the scattering cross sections can be computed.

5.1 Far Fields

The total radiated far-field in u-polarization can be computed from

$$E_u = \frac{j\omega\mu}{4\pi}\frac{e^{-jkr}}{r}\sum_{m,n} [\tilde{R}_m^u][Y_{m,n}][V_n], \quad u = \phi \text{ or } \theta \tag{42}$$

where the sum is taken over all modes m,n used in the analysis. In general, the far-field power radiated by a BOT, excited by an arbitrary antenna configuration, is given by

$$g_u = \frac{k^2\eta}{4\pi P_o} \left| \sum_{m,n} [\hat{R}^u_m][Y_{m,n}][V_n] \right|^2 , \qquad (43)$$

where

$$P_o = \sum_{m,n} \text{Re} \left\{ [\hat{V}_m][Y_{m,n}][V^*_n] \right\} ; \; \eta = \sqrt{\frac{\mu_o}{\varepsilon_o}} \qquad (44)$$

where the caret indicates a row vector. The matrix Y_{mn} denotes the partitioned submatrix corresponding to the (m,n)-th modes in the inverted Z_{BOT} matrix. The form of the excitation voltage vector V_n depends upon the type and location of the antenna on the BOT. As an example, consider a series of K aperture (slot) antennas embedded in the BOT surface and centered at (τ_k, ζ_k), k = 1, 2 . . . K. Assuming that the apertures are rectangular, then if the aperture at the i-th axial strip subtends one triangle function $f_i(\tau)$ and an axial width of $(\zeta_1 - \zeta_0)$,

$$V^\alpha_{ni} = \frac{1}{\Gamma L} \left\langle \vec{W}^\alpha_{ni}, \vec{E}_i \right\rangle$$

$$= \int_i d\tau \; f_i(\tau) \int_{\zeta_0}^{\zeta_1} d\zeta \; \vec{u}_\alpha \cdot \vec{E}_i(\tau,\zeta) \; e^{-jn\pi\zeta} , \; \alpha = t \text{ or } z \qquad (45)$$

In general, the aperture excitation function $\vec{E}_i(\tau,\zeta)$ can be specified to be of any form. For this discussion, let the slot be uniformly excited by E_i(V/m) in the α-polarization, so that

$$\vec{E}^\alpha_i = \vec{u}_\alpha \; E_i \begin{cases} 1 , & |\zeta| \le |\zeta_1 - \zeta_0| \\ 0 , & \text{otherwise} \end{cases} . \qquad (46)$$

Then

$$V^\alpha_{ni} = a_{ni} \; U^\alpha_i , \qquad (47)$$

where

$$U_i^{\alpha} = \int_i f_i(\tau)\, d\tau \tag{48}$$

and

$$a_{ni} = \begin{cases} (\zeta_1 - \zeta_0)\, E_i, & n = 0 \\ \dfrac{-1}{jn\pi}\left(e^{-jn\pi\zeta_1} - e^{-jn\pi\zeta_0}\right) E_i, & n \neq 0 \end{cases} \tag{49}$$

In the above expressions, it is assumed that the i-th slot is excited uniformly in the t and/or z polarization by an electric field, E_1, which may be a complex quantity. In the program if $V_{ni}^{\alpha} \neq 0$, then $(U^{\alpha})_i$ is represented by an array of the form

$$U = \begin{bmatrix} 0 \\ \vdots \\ U_i^t \\ \vdots \\ 0 \\ \hline 0 \\ \vdots \\ U_i^z \\ \vdots \\ 0 \end{bmatrix} \tag{50}$$

If the slots are excited solely in the t-polarization, then $U_i^z = 0$. For simplicity, U_i^t and U_i^z can be set equal to unity. By obvious extension, these results can be generalized for a BOT containing a series of slots at a given axial strip, as in the case of two-dimensional antenna arrays.

5.2 Scattered Fields

In general, the cross section in terms of the scattering geometry shown in Figure 6 is given as

$$\frac{\sigma^{pq}}{\lambda^2}(\theta_i, \phi_i, \theta_s, \phi_s) = \frac{k^2\eta^2}{4\pi\lambda^2} \left| \sum_{m,n} [\hat{R}^p_m][Y_{m,n}] \; [R^q_{-n}] \right|^2 , \qquad (51)$$

$$[R^p_m] = \begin{bmatrix} R^{tp}_m \\ R^{zp}_m \end{bmatrix} ,$$

where q and p denote the polarization of the incident and scattered fields; (θ_i, ϕ_i) and (θ_s, ϕ_s) are the incident and scattering angles, and the transfer matrices $R^{\alpha\beta}_m$ (α = t,z; β = p,q) express the relationships between the current on S and an observation point in free space. Examples of cross sections computed from this expression are given in Section 8.

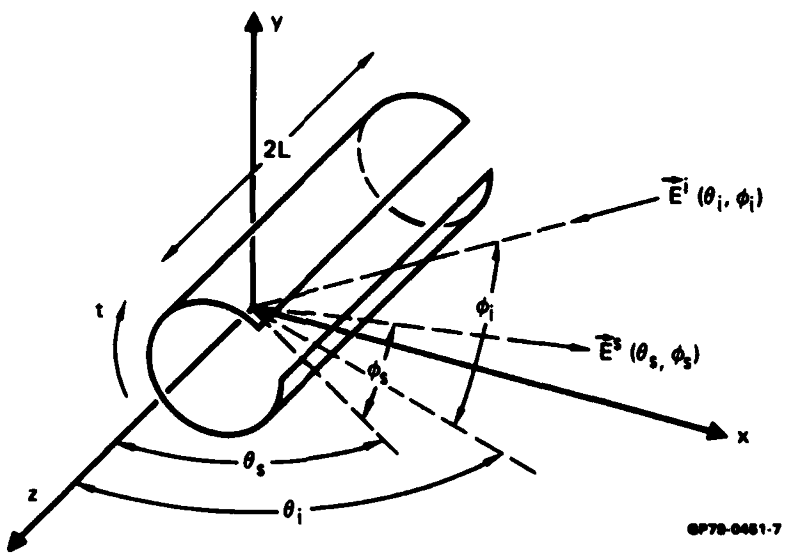

Figure 6. Coordinate geometry for scattering analysis.

6. NEAR-FIELD ANALYSIS

In the foregoing sections, the radiated and scattered fields were computed at field points sufficiently far from the BOT so that the wave fronts were planar and the field components transverse. Thus, the magnetic fields could be obtained from the computed electric fields via the free-space wave impedance, $\eta = 377\ \Omega$. In this section, the MM/BOT formulation is extended to permit the electric and magnetic fields to be computed at points $< \lambda$ distant from the BOT surface. First, the near-field expressions for the electric field will be derived, followed by the corresponding results for the magnetic field.

6.1 E-Near-Field Formulation

In general, the electric field at a free-space point r', resulting from a surface current density $\vec{J}$ on a surface S, is given by

$$\vec{E}(r') = L(\vec{J}), \tag{52}$$

where L(•) is the integro-differential operator defined in Equation (7). In this discussion, the current density can be induced by an incident wave illuminating the body as in a scattering problem or by an active aperture on S as in a radiation problem. The second term of $L(\vec{J})$ in Equation (7) can be rewritten using the relationship that

$$\nabla' \iint_S (\nabla \cdot \vec{J})\ \Phi(r - r')\ ds = \iint_S (\nabla \cdot \vec{J})\ (\vec{r} - \vec{r}')\ \Phi_1(r - r')\ ds,$$

where $\Phi_1(r - r') = [(1/R^2) + j(k/R)]\ \Phi(r - r')$ and $\Phi\ (r - r')$ is the free-space Green's function. If S corresponds to a BOT, the electric field at r' can be rewritten in terms of the t and z directed components of $\vec{J}$. Using the modal expansion for $\vec{J}$ [Equation (8)] in Equation (52),

$$\vec{E}(r') = j\omega\mu_o \Gamma L \sum_{n,j} \int_{-1}^{1} d\zeta \int_{j} d\tau \; e^{jn\pi\zeta} \; \Phi(r - r') \left[\vec{u}_t I^t_{nj} f^t_j(\tau) + \vec{u}_z I^z_{nj} f^z_j(\tau)\right]$$

$$- \frac{\Gamma L}{j\omega\epsilon_o} \sum_{n,j} \int_{-1}^{1} d\zeta \int_{j} d\tau \; e^{jn\pi\zeta} \; \Phi_1(r - r')\vec{B}(r - r') \tag{53}$$

$$\cdot \left[I^t_{nj} \frac{\dot{f}^t_j(\tau)}{\Gamma} + I^z_{nj} \left(\frac{jn\pi}{L}\right) f^z_j(\tau)\right],$$

where

$$\Phi(r - r') = \frac{e^{-jKR}}{4\pi RL} \tag{54}$$

$$\Phi_1(r - r') = \frac{1}{L^2}\left(\frac{1}{R^2} + \frac{jK}{R}\right)\Phi(r - r'), \tag{55}$$

$\vec{B}(r - r') = \vec{u}_x(x - x') + \vec{u}_y(y - y') + \vec{u}_z(z - z')$, and R is the distance between field and source points defined earlier. The evaluation of the integrals in the foregoing expression follows the schema used in determining the integrals in the impedance expressions [see Equations (13-15)]. Using a pulse approximation for the $f_i(\cdot)$ triangle functions, two generic integrals result with integrands containing $\Phi(r - r')$ and $\Phi_1(r - r')$. These are evaluated next. Denoting the field point r' with (τ_p, ζ'),

$$I_1 = \int_{-1}^{1} d\zeta \int_{j} d\tau \; e^{jn\pi\zeta} \; \Phi(r - r')$$

$$= e^{jn\pi\zeta'} \sum_{q=1}^{4} \int_{-1-\zeta'}^{1-\zeta'} d\xi \; e^{jn\pi\xi} \int_{q} d\tau \; \frac{e^{-jKR_p}}{4\pi LR_p}, \tag{56}$$

where $R_p = \sqrt{\delta^2 \rho_p^2 + \xi^2}$ with δ and ρ_p defined as before (Section 4.4). The τ integration is carried out analytically after the integrand is expanded in a Taylor series about R_{pq}. Then, I_1 becomes

$$I_1 = e^{jn\pi\zeta'} \sum_{q=1}^{4} \int_{-1-\zeta'}^{1-\zeta'} d\xi \; e^{jn\pi\xi} \frac{e^{-jKR_{pq}}}{4\pi L} \left\{ - jK(\tau_2 - \tau_1) \right.$$

$$\left. + (1 + jKR_{pq}) \frac{1}{\delta} \int_{s_1}^{s_2} \frac{ds}{\sqrt{s^2+d^2}} \right\} \tag{57}$$

$$= \frac{e^{jn\pi\zeta'}}{L} \sum_{q=1}^{4} G_n(q),$$

where

$$G_n(q) = \frac{2}{M} \sum_{\mu=0}^{M-1} u_n(\xi_\mu) \; f(\xi_\mu), \tag{58}$$

$$u_n(\xi_\mu) = \frac{e^{jn\pi\xi_\mu}}{4\pi}, \tag{59}$$

$$\xi_\mu = \frac{2\mu+1}{M} - 1 - \zeta', \tag{60}$$

and $f(\xi_\mu)$ and its associated parameters are as defined before in Equations (27-28). Note the evaluation of I_1 is similar to that of $G_{mn}(p,q)$, except in the present case there is only one surface integral to evaluate instead of two.

The evaluation of the integrals containing $\Phi_1(r - r')$ parallels the steps followed above. Specifically,

$$
\begin{aligned}
I_2(\gamma) &= \int_{-1}^{1} d\zeta \int_j d\tau \; e^{jn\pi\zeta} \, (\zeta - \zeta')^{\gamma} \, \Phi_1(r - r') \\
&= e^{jn\pi\zeta'} \sum_{q=1}^{4} \int_{-1-\zeta'}^{1-\zeta'} \xi^{\gamma} \, d\xi \int_q d\tau \; \frac{e^{-jKR_p}}{4\pi L R_p} \left(\frac{1}{R_p^{\,2}} + \frac{jK}{R_p} \right), \quad \gamma = 0 \text{ or } 1,
\end{aligned}
\tag{61}
$$

where $\xi = \zeta - \zeta'$. Expanding the integrand again about R_{pq}, the τ integration can be performed as before. The resulting expression for $I_2(\gamma)$ becomes

$$
I_2(\gamma) = \frac{e^{jn\pi\zeta'}}{L^3} \sum_{q=1}^{4} H_n^{\gamma}(q), \tag{62}
$$

where

$$
H_n^{\gamma}(q) = \frac{2}{M} \sum_{\mu=0}^{M-1} u_n^{\gamma}(\xi_\mu) \; h(\xi_\mu), \tag{63}
$$

$$
u_n^{o}(\xi_\mu) = \frac{e^{jn\pi\xi_\mu}}{4\pi}, \tag{64}
$$

$$
u_n^{1}(\xi_\mu) = \xi_\mu \; u_n^{o}(\xi_\mu), \tag{65}
$$

and

$$
\begin{aligned}
h(\xi_\mu) = \frac{e^{-jKR_{pq}}}{\delta} \Bigg\{ & K^2 \chi - \frac{K^2 R_{pq}}{d} \left[\tan^{-1}\left(\frac{s_2}{d}\right) - \tan^{-1}\left(\frac{s_1}{d}\right) \right] \\
& + \frac{(1 + jKR_{pq})}{d^2} \left[\frac{s_2}{\sqrt{s_2^2 + d^2}} - \frac{s_1}{\sqrt{s_1^2 + d^2}} \right] \Bigg\},
\end{aligned}
\tag{66}
$$

where χ and all the other parameters have been defined before. The expressions for I_1 and I_2 have no self-terms since the point of observation $r'(= r_p)$ is assumed to be different than r, i.e., $R_{pq} \neq 0$.

Using the results for I_1 and I_2, the expression for the electric field in terms of the G and H functions become

$$
\begin{aligned}
\vec{E}(r') = 2jk\eta\, e^{jn\pi\zeta'} \Bigg\{ & \vec{u}_x \Gamma \Bigg[\sum_{n,j} I_{nj}^{t} \sum_{q=1}^{4} \left(T_q^t \cos\nu_q \, G_n(q) + \frac{1}{\Gamma K^2} \dot{T}_q^t (x_q - x') \, H_n^o(q) \right) \\
& + \sum_{n,j} I_{nj}^{z} \left(\frac{jn\pi\delta}{\Gamma K^2} \right) \sum_{q=1}^{4} T_q^z (x_q - x') \, H_n^o(q) \Bigg] \\
& + \vec{u}_y \Gamma \Bigg[\sum_{n,j} I_{nj}^{t} \sum_{q=1}^{4} \left(T_q^t \sin\nu_q \, G_n(q) + \frac{1}{\Gamma K^2} \dot{T}_q^t (y_q - y') \, H_n^o(q) \right) \qquad (67) \\
& + \sum_{n,j} I_{nj}^{z} \left(\frac{jn\pi\delta}{\Gamma K^2} \right) \sum_{q=1}^{4} T_q^z (y_q - y') \, H_n^o(q) \Bigg] \\
& + \vec{u}_z \Gamma \sum_{n,j} \Bigg[I_{nj}^{z} \sum_{q=1}^{4} T_q^z \left(G_n(q) + \frac{jn\pi}{K^2} H_n^1(q) \right) + I_{nj}^{t} \sum_{q=1}^{4} \frac{\dot{T}_q^t H_n^1(q)}{K^2 \delta} \Bigg] \Bigg\}.
\end{aligned}
$$

6.2 H-Near-Field Formulation

In general, the magnetic field is given in terms of the vector potential $\vec{A}$ and the incident field $\vec{H}^i(r')$ as

$$\vec{H}(r') = \vec{H}^i(r') + \nabla' \times \vec{A}(r'), \qquad (68)$$

where the primed coordinate is at an arbitrary test point where the field is to be sampled. Letting $\vec{H}^i(r') = 0$, since there is no field at r', except that caused by currents induced on the scattering or radiating surface S, Equation (68) becomes

$$\vec{H}(r') = \nabla' \times \iint_S \vec{J}(r)\ \Phi(r - r')\ ds$$

$$= -\iint_S \vec{J}(r) \times \nabla'\ \Phi(r - r')\ ds. \tag{69}$$

Expanding the gradient over the unprimed coordinates,

$$\nabla'\ \Phi(r - r') = (\vec{r} - \vec{r}')\ \Phi_1(r - r'),$$

where $\Phi(r - r')$ and $\Phi_1(r - r')$ were defined before in the E-near-field analysis. Noting that the surface current density on the BOT may be decomposed into t and z components, Equation (69) can be written explicitly as

$$\vec{H}(r') = -\iint_S \Big\{ \vec{u}_x \Big[(z - z')\sin\nu\ J_t - (y - y')J_z\Big] + \vec{u}_y \Big[(x - x')J_z - (z - z')\cos\nu\ J_t\Big] + \vec{u}_z \Big[(y - y')\cos\nu\ J_t - (x - x')\sin\nu\ J_t\Big]\Big\}\ \Phi_1. \tag{70}$$

Using the modal expansion of the current components [Equation (8)] and evaluating the surface integrals in the same manner as in the E-near-field analysis, yields the following expression for $\vec{H}(r')$:

$$\vec{H}(r') = -2\ e^{jn\pi\zeta'} \Bigg\{ \vec{u}_x \Bigg[\delta \sum_{n,j} \Bigg(I^t_{nj} \sum_{q=1}^{4} T^t_q \sin\nu_q\ H^1_n(q) - \Gamma\delta^2\ I^z_{nj} \sum_{q=1}^{4} T^z_q (y_q - y')H^o_n(q)\Bigg)\Bigg] + \vec{u}_y \Bigg[-\delta \sum_{n,j} \Bigg(I^t_{nj} \sum_{q=1}^{4} T^t_q \cos\nu_q\ H^1_n(q) + \Gamma\delta^2\ I^z_{nj} \sum_{q=1}^{4} T^z_q (x_q - x')H^o_n(q)\Bigg)\Bigg] + \vec{u}_z \Bigg[\Gamma\delta^2 \sum_{n,j} I^t_{nj} \sum_{q=1}^{4} T^t_q \Big((y_q - y')\cos\nu_q - (x_q - x')\sin\nu_q\Big) H^o_n(q)\Bigg]\Bigg\}. \tag{71}$$

The spherical field components at $r'(= \rho', \phi', \theta')$ for the E and H fields can be formed by combining the cartesian components in Equations (67) or (71). Thus, letting $\vec{A}$ denote the $\vec{E}$ or $\vec{H}$ fields, the appropriate spherical field components are given by:

$$A_{\theta'} = A_x \cos\theta' \cos\phi' + A_y \cos\theta' \sin\phi' - A_z \sin\theta' \tag{72}$$

$$A_{\phi'} = - A_x \sin\phi' + A_y \cos\phi' \tag{73}$$

$$A_{\rho'} = A_x \cos\phi' + A_y \sin\phi'. \tag{74}$$

In the foregoing discussion, the electric and magnetic near-fields were sampled at a point. An alternate approach was also considered in which the fields were sampled and averaged over a rectangular patch. This latter formulation was a generalization of that given in Reference (17). The predictions from the patch and point near-field analyses were compared for a number of BOT configurations. Numerical simulation showed that in regions where the electromagnetic wave departs significantly from being planar (i.e., in the vicinity of active or passive apertures), the point-sampled fields were more accurate, particularly for aperture-coupled fields. Actual comparison of these formulations is detailed in Section 8.

7. APERTURE COUPLED FIELDS

The problem of electromagnetic fields penetrating through small apertures has been treated previously using the Bethe small hole theory.[18-21] Recently, the MM technique has been applied to symmetric and asymmetric apertures in BOR.[22,24] A computer program has been developed by Schuman[22] to treat the former class of problems. Here, the MM technique is applied to the case of rectangular asymmetric apertures embedded in the BOT. The analysis uses the Schelkunoff equivalence theorem, which replaces the external sources illuminating a body with apertures with an equivalent problem having only aperture current sources. From the aperture currents, the near fields inside the body can be computed. In the present discussion, the aperture is assumed to lie anywhere on the BOT surface; however, an aperture near the ends of the BOT can lead to anomalous unphysical results. The aperture edges are taken to lie parallel to the z and t coordinates of the BOT, a restriction that can be relaxed at a cost of greater analytical complexity. The subsequent discussion assumes a single aperture. The extension of the analysis to several apertures is straightforward. The Schelkunoff equivalence theorem[25] is discussed next for a general scattering surface, followed by its application to a BOT.

7.1 Schelkunoff Equivalence Theorem

A graphical statement of this theorem is shown in Figure 7. The original problem of external fields $\vec{E}$ and $\vec{H}$ illuminating a body with an aperture is depicted in Figure 7a. The internal (aperture coupled) fields are $\vec{E}_2$ and $\vec{H}_2$. With the aperture covered (Figure 7b), a current $\vec{J}^o$ is induced in the region of the covered aperture as a result of the external fields $\vec{E}_1^o$ and $\vec{H}_1^o$. In Figure 7c, the equivalent current in the aperture region is shown as $(-J^o)$ because of the composite external electric and magnetic fields, i.e., $(\vec{E}_1 - \vec{E}_1^o)$ and $(\vec{H}_1 - \vec{H}_1^o)$, respectively. A simple superposition of the problem depicted in Figures 7b and 7c yields the original problem in Figure 7a. The results of the Schelkunoff theorem will be applied to a BOT geometry in the following section.

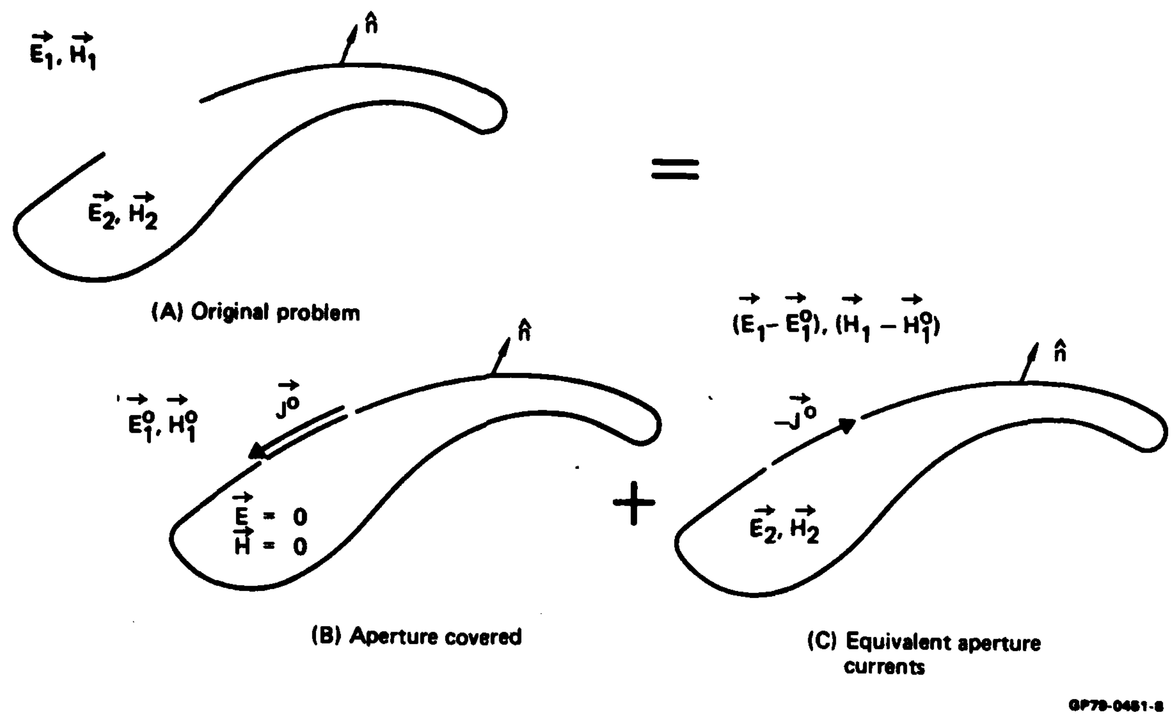

Figure 7. Schelkunoff's equivalence theorem.

7.2 Expansion of the Aperture Voltage

Assume that a rectangular aperture is centered at τ_α and ζ_α on the BOT (Figure 8). (The normalization of the coordinates adopted in Section 4.1 is again used.) Let the BOT surface be illuminated by a plane wave ($\vec{E}_1$, $\vec{H}_1$) eminating from an angle (θ_1, ϕ_1). Then the field in V/m at the q-th strip spanned by the j-th triangle function $f_j(\tau)$ subtending the aperture is

$$\vec{E}_q = \left(\vec{u}_t\ A^t_q\ X^t_q(\tau) + \vec{u}_z\ A^z_q\ X^z_q(\tau)\right)\ U\left(|\zeta - \zeta_\alpha| \le \frac{\Delta\zeta}{2}\right)\ , \qquad (75)$$

where

$$\Delta\zeta = |\zeta_1 - \zeta_0|$$

and A^t_q and A^z_q are the t and z-polarized field components induced across the aperture are due to the incident fields. These components will be determined

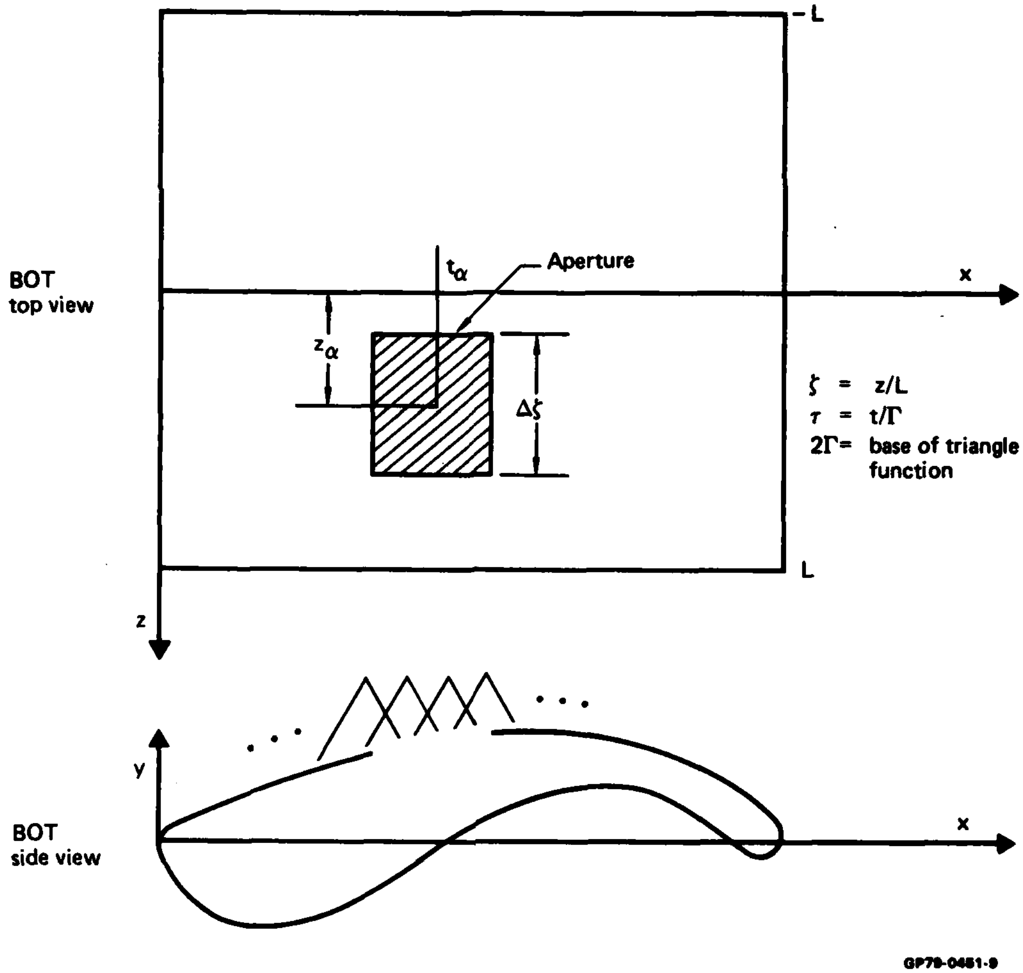

Figure 8. BOT geometry for aperture analysis.

in terms of the illuminating plane-wave incident on the entire BOT surface. In Equation (75), U(·) is the unit pulse function and $X_q^\alpha(\tau)$, (α = t or z) is the sampling function of the fields in the aperture. In this formulation, these components are defined to be pulse functions (Figure 9) and are similar to those used by Schuman in the MM/BOR analysis[22]. Note the $X_q^\alpha(\cdot)$ functions are modified near the ends of the aperture to approximate the edge behavior of the t- and z-directed currents. If the aperture subtends N strips, then Equation (75) is generalized so that the total aperture field is

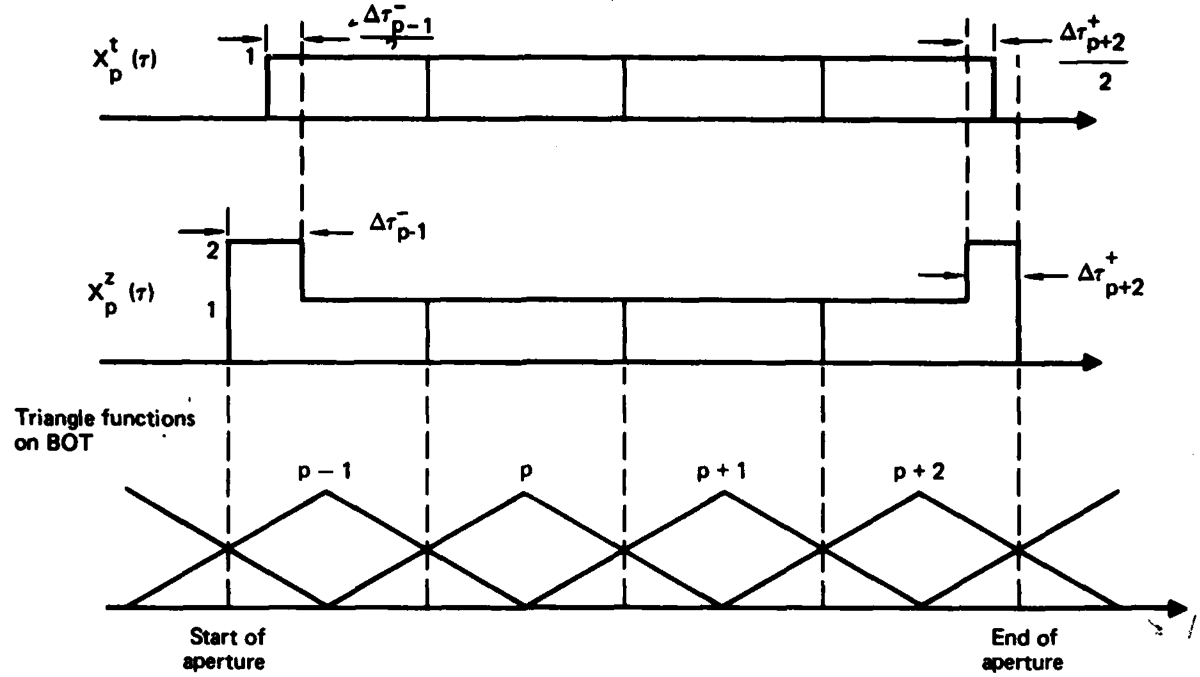

Figure 9. Representation of expansion functions in aperture region.

$$\vec{E} = \sum_{q=1}^{N} \vec{E}_q \ . \tag{76}$$

The induced voltage at the aperture [Equation (75)] can be expanded in terms of the expansion functions used previously on the BOT, i.e.,

$$\vec{E}_q = \sum_n \left\{ \vec{u}_t \ V^t_{nj} \ f^t_j(\tau) + \vec{u}_z \ V^z_{nj} \ f_j(\tau) \right\} e^{jn\pi\zeta} \ . \tag{77}$$

Equating Equations (75) and (77),

$$\begin{aligned} V^\alpha_{nj} &= \left\langle \vec{u}_\alpha \ f^\alpha_j(\tau) \ e^{-jn\pi\zeta}, \ \vec{u}_\alpha \ A^\alpha_q \ X^\alpha_q(\tau) \ U(\cdot) \right\rangle \\ &= A^\alpha_q \ D_n \ F^\alpha_{j,q} \ , \end{aligned} \tag{78}$$

where

$$\left.\begin{matrix}\zeta_2\\ \zeta_1\end{matrix}\right\} = \zeta_\alpha \pm \frac{\Delta\zeta}{2}$$

$$D_n = \Delta\zeta \; e^{-jn\pi\zeta_\alpha} \; \mathrm{sinc}\left(\frac{n\pi\Delta\zeta}{2}\right) \tag{79}$$

and

$$F^\alpha_{j,q} = \int_{\tau^-}^{\tau^+} d\tau \; f^\alpha_j(\tau) \; X^\alpha_q(\tau) \; . \tag{80}$$

The limits of integration τ^+ and τ^- span the opening of the aperture in the τ direction. If the pulse function $X^\alpha_q(\cdot)$ also overlaps the $(j \pm 1)$-th triangle functions, then Equation (80) also yields $F^\alpha_{j\pm1,q}$.

For a given illuminating field $\vec{E}$, in either θ or ϕ polarization, the voltage vector V_n is specified so that the currents on the BOT can be computed on the surface with the aperture covered over (i.e., Figure 7b) from

$$\begin{bmatrix} I_{-n} \\ \vdots \\ I_o \\ \vdots \\ I_n \end{bmatrix} = \begin{bmatrix} & & \\ & Z_{BOT} & \\ & & \end{bmatrix}^{-1} \begin{bmatrix} V_{-n} \\ \vdots \\ V_o \\ \vdots \\ V_n \end{bmatrix} \quad (\mathrm{A/m}) \; , \tag{81}$$

$$V_n] = \begin{bmatrix} \begin{bmatrix} V^t_{n,1} \\ \cdot \\ \cdot \\ \cdot \\ V^t_{n,I} \end{bmatrix} \\ \\ \begin{bmatrix} V^z_{n,1} \\ \cdot \\ \cdot \\ \cdot \\ V^z_{n,I} \end{bmatrix} \end{bmatrix} \quad (\mathrm{V/m}) \tag{82}$$

$$\left.\begin{matrix} 0 \\ \cdot \\ \cdot \\ \cdot \\ 0 \\ V^\alpha_{n,j-1} \\ V^\alpha_{n,j} \\ V^\alpha_{n,j+1} \\ 0 \\ \cdot \\ \cdot \\ \cdot \\ 0 \end{matrix}\right] = \begin{bmatrix} 0 \\ \cdot \\ \cdot \\ \cdot \\ 0 \\ D_n A^\alpha_q \begin{Bmatrix} F^\alpha_{j-1,q} \\ F^\alpha_{j,q} \\ F_{j-1,q} \end{Bmatrix} \\ 0 \\ \cdot \\ \cdot \\ \cdot \\ 0 \end{bmatrix} \; ; \; (\alpha = t \text{ or } z) \, . \tag{83}$$

7.3 Derivation of the Aperture Admittance

Equation (81) yields a relationship between the modal current components on the BOT corresponding to the i-th triangle function (i.e., I_{ni}, n = 0, ± 1, ...) because of a voltage sampled by the j-th triangle function (i.e., V_{nj}). Writing out Equation (81) explicitly with only the i-th rows and j-th columns retained,

$$
\begin{bmatrix}
\begin{bmatrix} I^t_{-ni} \\ I^z_{-ni} \end{bmatrix} \\
\vdots \\
\begin{bmatrix} I^t_{oi} \\ I^z_{oi} \end{bmatrix} \\
\vdots \\
\begin{bmatrix} I^t_{ni} \\ I^z_{ni} \end{bmatrix}
\end{bmatrix}
=
\begin{bmatrix}
\begin{bmatrix} y^{tt}_{ij} & y^{tz}_{ij} \\ y^{zt}_{ij} & y^{zz}_{ij} \end{bmatrix}_{-n,-n} & & \cdot^{\cdot^{\cdot}} \\
& \ddots \begin{bmatrix} y^{tt}_{ij} & y^{tz}_{ij} \\ y^{zt}_{ij} & y^{zz}_{ij} \end{bmatrix}_{o,o} \ddots & \\
\cdot^{\cdot^{\cdot}} & & \begin{bmatrix} y^{tt}_{ij} & Y^{tz}_{ij} \\ y^{zt}_{ij} & y^{zz}_{ij} \end{bmatrix}_{n,n}
\end{bmatrix}
\begin{bmatrix}
\begin{bmatrix} V^t_{-nj} \\ V^z_{-nj} \end{bmatrix} \\
\vdots \\
\begin{bmatrix} V^t_{oj} \\ V^z_{oj} \end{bmatrix} \\
\vdots \\
\begin{bmatrix} V^t_{nj} \\ V^z_{nj} \end{bmatrix}
\end{bmatrix}
\qquad (84)
$$

For the subsequent discussion, it is convenient to adopt the following shorthand notation for Equation (84). The m-th row of Equation (84) can be written as:

$$
\begin{bmatrix} I^t_{mi} \\ I^z_{mi} \end{bmatrix} = \left[\sum_n \left(Y_{ij} \right)_{mn} \right] \begin{bmatrix} V^t_{nj} \\ V^z_{nj} \end{bmatrix} \quad , \; m = 0, \pm 1, \ldots \; , \qquad (85)
$$

where $\left(Y_{ij} \right)_{mn}$ denotes the individual partitioned submatrices in Equation (84). The admittance matrix in Equation (84) is a full matrix with all m,n modes included. If the sampling points p and q lie within the aperture boundary, then the above admittance matrix of the apertureless BOT can be related to the admittance of the aperture. This case is considered next.

Formally, the currents C_{ap} in the region corresponding to the p-th sampling function X_p in the covered aperture region can be expressed as

$$
\begin{bmatrix} C^t_{ap} \\ C^z_{ap} \end{bmatrix} = \left[\begin{array}{c|c} \left(Y^{tt}_a \right)_{pq} & \left(Y^{tz}_a \right)_{pq} \\ \hline \left(Y^{zt}_a \right)_{pq} & \left(Y^{zz}_a \right)_{pq} \end{array} \right] \begin{bmatrix} A^t_q \\ A^z_q \end{bmatrix} \qquad (86)
$$

$$= - f_p \sum_m e^{jm\pi\zeta_p} \begin{bmatrix} I^t_{mi} \\ I^z_{mi} \end{bmatrix} , \tag{86a}$$

where the currents C_{ap} are expanded in terms of modal components and triangle functions, where the aperture admittance $\left(Y_a\right)_{pq}$ is determined in terms of $\left(Y_{ij}\right)_{mn}$, and where A^t_q and A^z_q are the t- and z-polarized field components across the aperture (see Equation 75). The negative sign in Equation (86a) is due to the Schelkunoff theorem, i.e., the equivalent aperture currents are the negative of the currents induced on the apertureless body in the vicinity of the aperture resulting from the illuminating fields (i.e., Figure 7c). Substituting Equation (85) into Equation (86a) and using the results of Equation (83),

$$\begin{bmatrix} C^t_{ap} \\ C^z_{ap} \end{bmatrix} = - f_p \sum_m e^{jm\pi\zeta_p} \sum_n \left(Y_{ij}\right)_{mn} \begin{bmatrix} V^t_{nq} \\ V^z_{nq} \end{bmatrix} \tag{87}$$

$$= - f_p \sum_m e^{jm\pi\zeta_p} \sum_n D_n \left\{ \left(Y^{\alpha\beta}_{ij}\right)_{mn} F^{\beta}_{j-1,q} \right.$$

$$\left. + \left(Y^{\alpha\beta}_{ij}\right)_{mn} F^{\beta}_{j,q} + \left(Y^{\alpha\beta}_{ij}\right)_{mn} F^{\beta}_{j+1,p} \right\} \begin{bmatrix} A^t_q \\ A^z_q \end{bmatrix} , \tag{87a}$$

where $\left(Y^{\alpha\beta}_{kl}\right)_{m,n}$ is the (k,l)-th element of the entire inverted Z_{BOT} matrix for mode pair (m,n), and α,β denotes tt, tz, zt, or zz. The bracketed terms in Equation (87a) constitute a matrix partitioned like Y_a in Equation (86). The expression for the individual elements of the admittance matrix is obtained by equating the right sides of Equations (86) and (87a), i.e.,

$$\left(Y_a^{\alpha\beta}\right)_{pq} = -\ell_p \sum_{m,n} e^{jm\pi\zeta_p} D_n \left\{ \left(Y_{i,j-1}^{\alpha\beta}\right)_{mn} F_{j-1,q}^{\beta} \right.$$

$$\left. + \left(Y_{i,j}^{\alpha\beta}\right)_{mn} F_{j,q}^{\beta} + \left(Y_{i,j+1}^{\alpha\beta}\right)_{mn} F_{j+1,q}^{\beta} \right\}, \tag{88}$$

where D_n and F^{α} are given in Equations (79) and (80), respectively. Thus, the individual elements of the aperture admittance are composed of a triplet of matrix elements from the inverted Z_{BOT} modified by the integral of the aperture sampling functions, represented by the F functions. The above expression is the admittance of an asymmetric aperture and is generically similar to the BOR results given in Reference 22 for the circumferentially symmetric aperture problem.

7.4 Equivalent Aperture Excitation Voltage

To compute the aperture coupled fields (i.e., $\vec{E}_2$ and $\vec{H}_2$ in Figure 7c), the voltage induced in the aperture as a result of the illuminating fields must be computed. This voltage is the equivalent aperture excitation voltage which can be obtained from the aperture admittance and the currents in the aperture region. For the p-th current C_{ap}^{α} (α = t or z), the equivalent aperture voltage EV_q^{α}, sampled by $X_q^{\alpha}(\cdot)$ is given by

$$\begin{bmatrix} EV_q^t \\ EV_q^z \end{bmatrix} = \left[\begin{array}{c|c} \left(Y_a^{tt}\right)_{pq} & \left(Y_a^{tz}\right)_{pq} \\ \hline \left(Y_a^{zt}\right)_{pq} & \left(Y_a^{zz}\right)_{pq} \end{array}\right]^{-1} \begin{bmatrix} C_{ap}^t \\ C_{ap}^z \end{bmatrix} \qquad p = 1, \ldots K, \tag{89}$$

where K denotes the number of pulse-sampling functions $X_p(\cdot)$ used to describe the current in the aperture region. Having determined EV_q^{α} (q = 1, . . . K), the voltage excitation V_{nj}^{α} corresponding to the j-th triangle function on the original BOT spanning $X_p(\cdot)$ can be obtained from

$$\begin{bmatrix} V^t_{mj} \\ V^z_{mj} \end{bmatrix} = D_n \left[\begin{array}{c} EV^t_p \; (F^t_{j-1,p} + F^t_{j,p} + F^t_{j+1,p}) \\ \hdashline EV^z_p \; (F^z_{j-1,p} + F^z_{j,p} + F^z_{j+1,p}) \end{array}\right] . \tag{90}$$

Then the effective currents on the BOT in the presence of the aperture for the m-th mode and the i-th triangle function are given by:

$$\begin{bmatrix} C^t_{ni} \\ C^z_{ni} \end{bmatrix} = \sum_{m,j} \left[\begin{array}{c:c} \left(Z^{tt}_{ij}\right)_{mn} & \left(Z^{tz}_{ij}\right)_{mn} \\ \hdashline \left(Z^{zt}_{ij}\right)_{mn} & \left(Z^{zz}_{ij}\right)_{mn} \end{array}\right]^{-1} \begin{bmatrix} V^t_{mj} \\ V^z_{mj} \end{bmatrix} , \tag{91}$$

where the indexes m and j run over all the modes and triangle functions on the BOT, respectively. The resulting total currents on the BOT with an aperture is reconstructed from the modal coefficients so that at the i-th sample point τ_i, the current is

$$\begin{bmatrix} C^t_i \\ C^z_i \end{bmatrix} = \sum_n \left\{ f_i(\tau) \; e^{jn\pi\zeta} \begin{bmatrix} C^t_{ni} \\ C^z_{ni} \end{bmatrix} \right\} . \tag{92}$$

The axial distribution of the currents is obtained by evaluating Equation (92) for $|\zeta| < 1$. At the edge $|\zeta| = 1$, theoretically, an infinite number of modes is required to obtain an accurate representation of the current. Since only a finite number of modes can be used in practical application of the MM/BOT formulation, care must be taken to interpret the current distribution near an edge.

7.5 Computation of Aperture-Coupled Fields

The electric and magnetic fields penetrating an aperture (i.e., $\vec{E}_2$ and $\vec{H}_2$ in Figure 7c) can be determined using the near-field formalism described

in Section 6. The aperture-coupled electric and magnetic fields are given by Equations (67) and (71), respectively, where the current coefficients I^{α}_{nj} are replaced by C_{nj} given by Equation (91), and the observation point r' is within the BOT. The three components ρ, ϕ, θ for the electric and magnetic fields are again obtained from Equations (72-74).

8. VALIDATION OF THE MM/BOT FORMULATION

The MM/BOT analysis was applied to compute the far fields radiated and scattered by a BOT as well as the near fields and aperture-coupled fields for various antenna, aperture, and body configurations. The results were compared with data obtained using accepted experimental or other theoretical methods. In the subsequent examples, the results for the scattering cross sections, near fields, and aperture-coupled fields are not normalized.

8.1 Validation of Far-Field Analysis

Because of the availability of computer codes for the MM/BOR formulation,[17] the far-field radiation patterns were computed for antennas embedded in a BOR. The results from the MM/BOR and MM/BOT formulations were compared. As an example, a slot antenna embedded in a right cylinder of radius 0.216 λ and length 2.76 λ is depicted in Figure 10. The ϕ-polarized slot subtends an angle of 45° and is 2.06 λ long. The pitch (vertical) and roll plane power radiation patterns are plotted in linear power, normalized to the MM/BOR results. There is excellent agreement between the MM/BOR and MM/BOT results, with seven circumferential and four axial modes being used in the respective calculations. The sensitivity of the MM/BOT calculated pitch and roll plane patterns for the above slotted cylinder as a function of modal sparsing is shown in Figures 11 and 12, respectively. The calculations show that use of only diagonal modes (i.e., m = n) in the MM/BOT results in an approximate 10% deviation from the MM/BOR patterns. The power distribution, normalized to an isotropic radiator, versus mode number is shown in Figure 13 for this problem. (The numbers in parentheses are exponents. "Negative" powers arise from computer round-off errors and are insignificantly small. Negative powers are often also obtained for certain modes in the MM/BOR analysis of Mautz and Harrington.) The maximum powers occur in the self-modes (i.e., m = n).

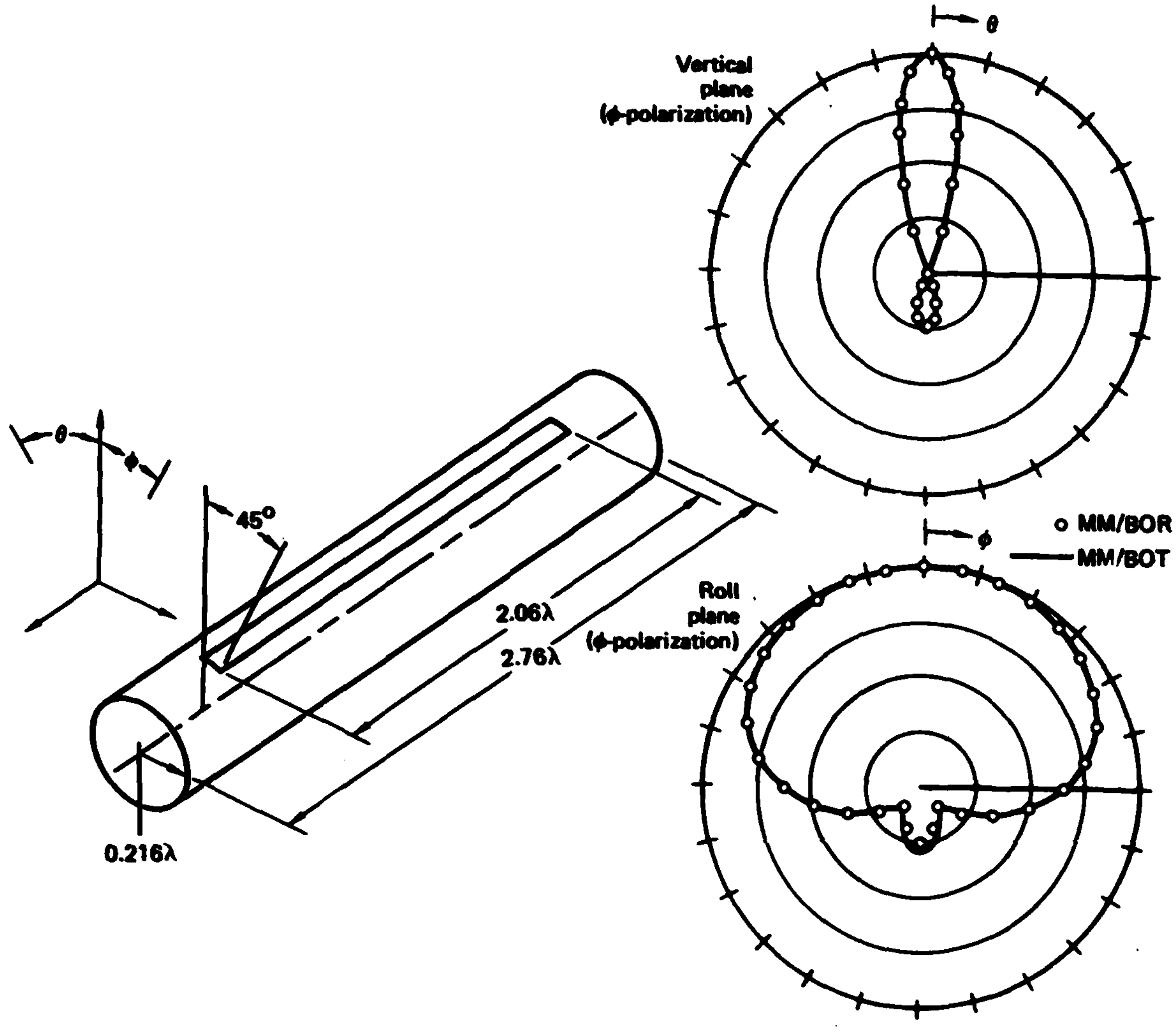

Figure 10. Comparison of MM/BOR and MM/BOT computed power radiation patterns for a slotted cylinder (ϕ-polarized slot).

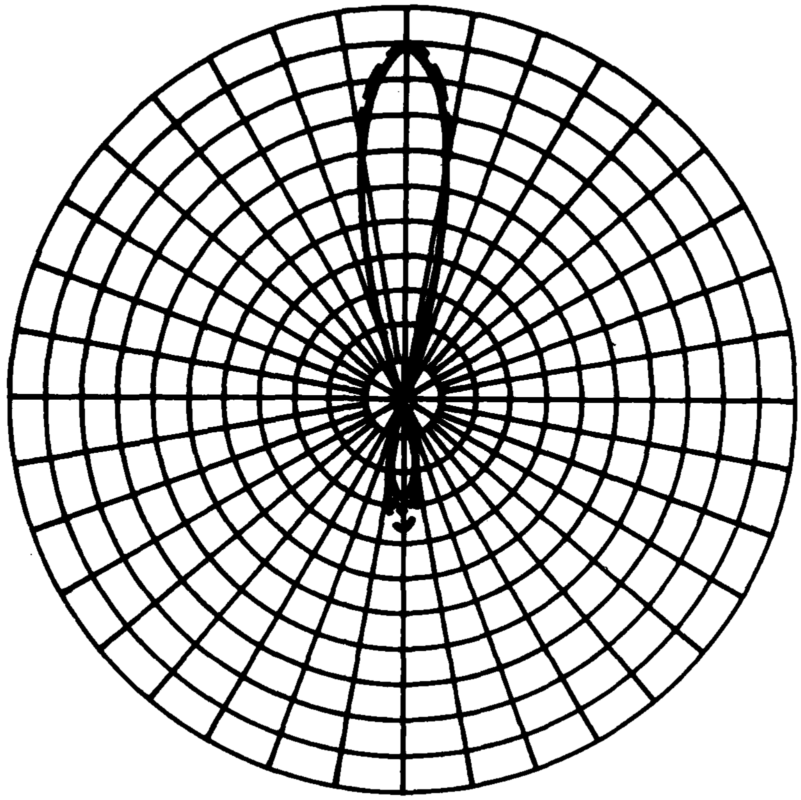

MM/BOT, 4 modes
MM/BOT, main diagonal modes
MM/BOT, main and off-diagonal modes

2.76 λ long BOR
ka = 1.35

Slot dimensions:
2.06 λ x 0.084 λ

GP79-0451-12

Figure 11. Sensitivity of radiation patterns to modal sparsing: vertical plane (ϕ-fed axial slot).

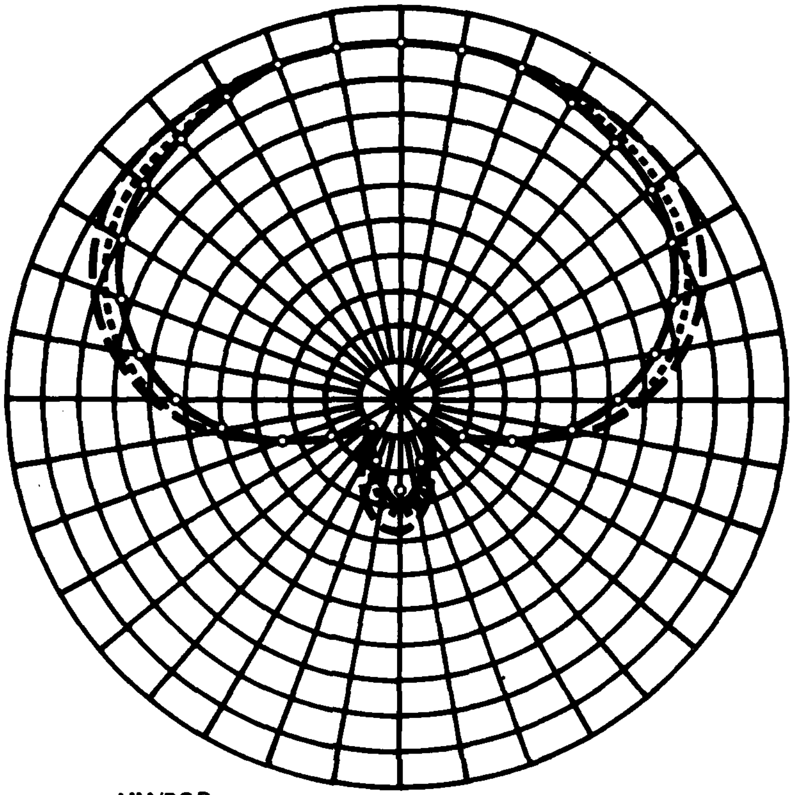

o MM/BOR
———— MM/BOT, 4 modes
— — — MM/BOT, main diagonal modes
.... MM/BOT, main and off-diagonal modes

Slot dimensions:
2.06λ x 0.084λ

2.76 λ long BOR
ka = 1.35

GP79-0451-83

Figure 12. Sensitivity of radiation patterns to modal sparsing: roll plane (ϕ-fed axial slot).

m \ n	−3	−2	−1	0	1	2	3
−3	4.08(−6)						
−2	7.2(−6)	7(−5)			ϕ - fed slot: 2.06λ x 0.084λ		
−1	1.2(−5)	3.2(−5)	2.6(−4)				
0	−4.8(−5)	−1.3(−4)	−2.2(−4)	3.4(−3)			
1	1.6(−5)	4.6(−5)	6.7(−5)	−2.2(−4)	2.6(−4)		
2	1.1(−5)	3.4(−5)	1.6(−5)	−1.3(−4)	3.1(−5)	7 (−5)	
3	2.2(−6)	1.1(−5)	−4.8(−5)	−4.8(−5)	1.2(−5)	7.2(−6)	4(−6)

GP79-0461-13

Figure 13. Power distribution as a function of mode number (MM/BOT analysis for open cylinder 2.76 λ length, 0.216λ radius with ϕ - fed slot).

Examples validating the scattering analysis in Section 5.2 are considered next. In Figure 14, the bistatic scattering cross section for an open cylinder of radius 0.216 λ and length 2.16 λ is given. The cylinder is illuminated broadside ($\theta = 90°$) with a TE wave. The absolute cross sections predicted by the MM/BOR and MM/BOT formulations are in close agreement. The monostatic cross section for a square cross-sectioned cylinder when illuminated by a TM (θ-polarized) field is shown in Figure 15. The MM/BOT results are computed for a 2.76 λ long cylinder; the Wilton-Mittra data (Reference 8) are for the corresponding infinitely long cylinder.

The applicability of the present analysis is to degenerate BOT surfaces is demonstrated in Figures 16 and 17, where the monostatic scattering cross sections for a flat plate (2 λ on a side) and the bistatic cross section for a parabolic cylinder of 2.76 λ length are depicted. In both cases, the surfaces are illuminated broadside (i.e., $\phi_i = 0$, $\theta_i = 90$). For these calculations, 4 modes and 16 triangle functions were used. The MM/BOT results in Figure 16 are in good agreement with the experimental results of Ross.[26] Similarly, the TM polarized results for the finite-length parabolic cylinder in Figure 17 are in good agreement with the analytical predictions of Andreasen.

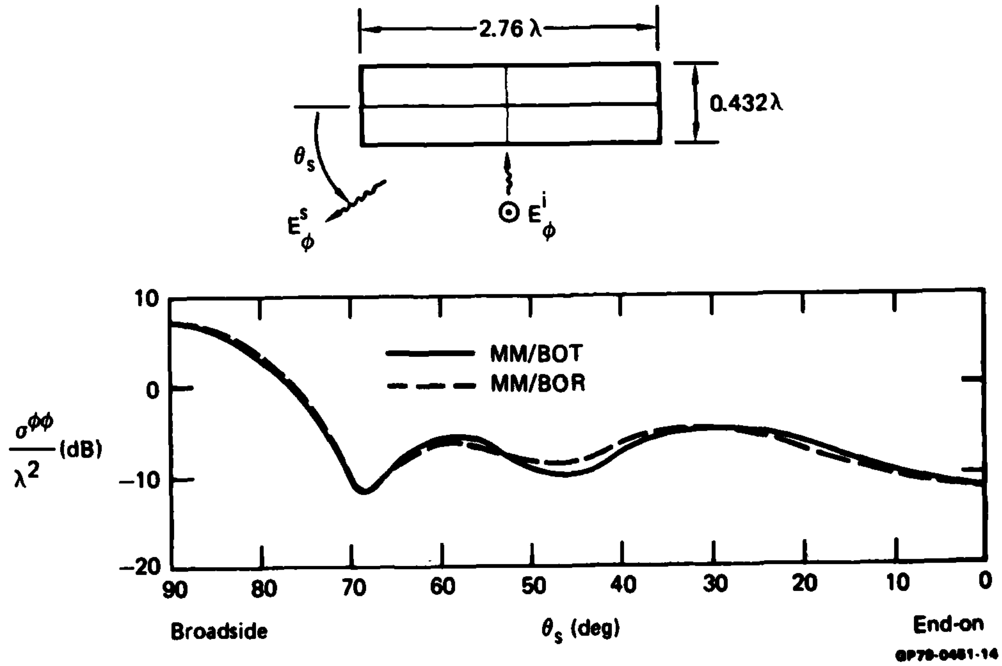

Figure 14. Comparison of MM/BOR and MM/BOT computed bistatic cross section for open cylinder.

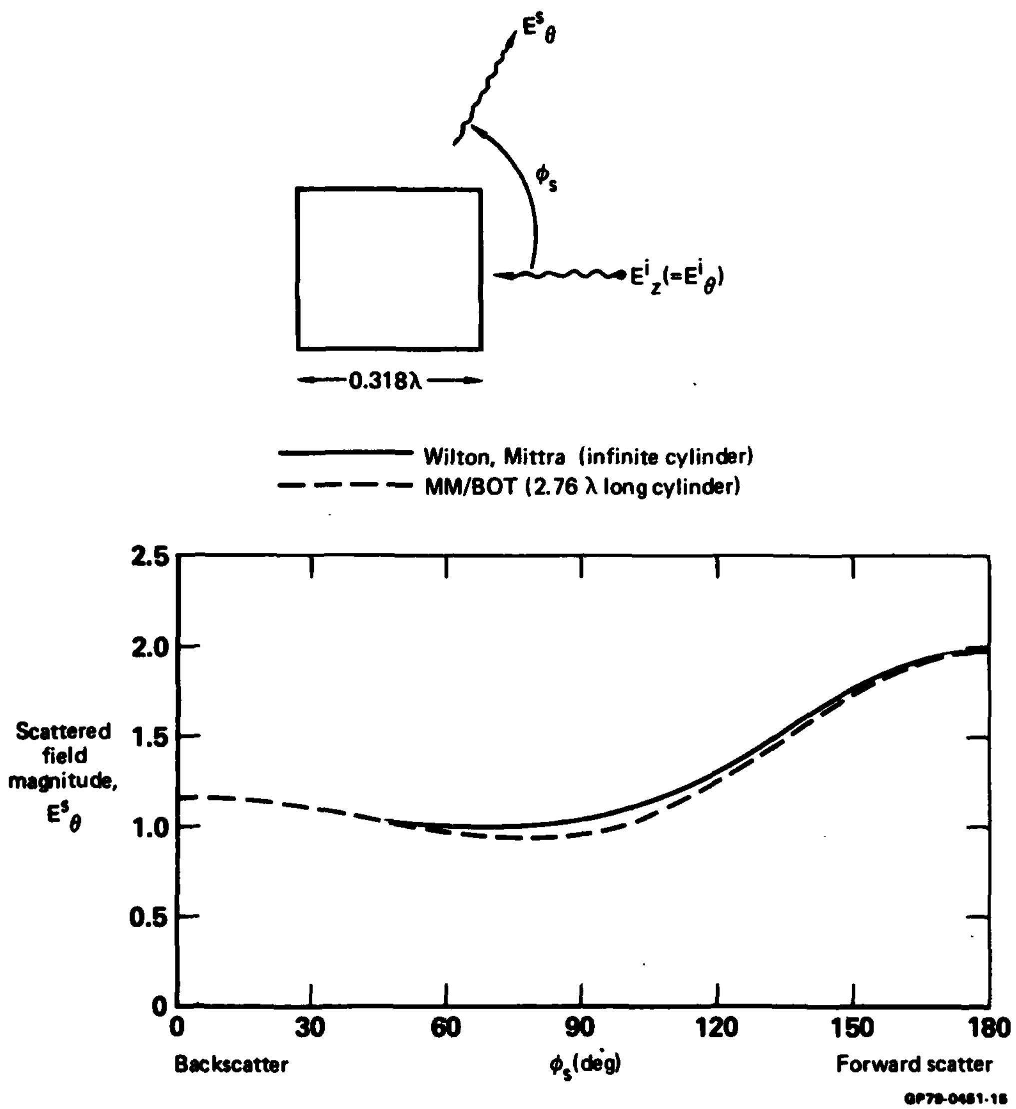

Figure 15. Bistatic scattering calculations for a square cylinder.

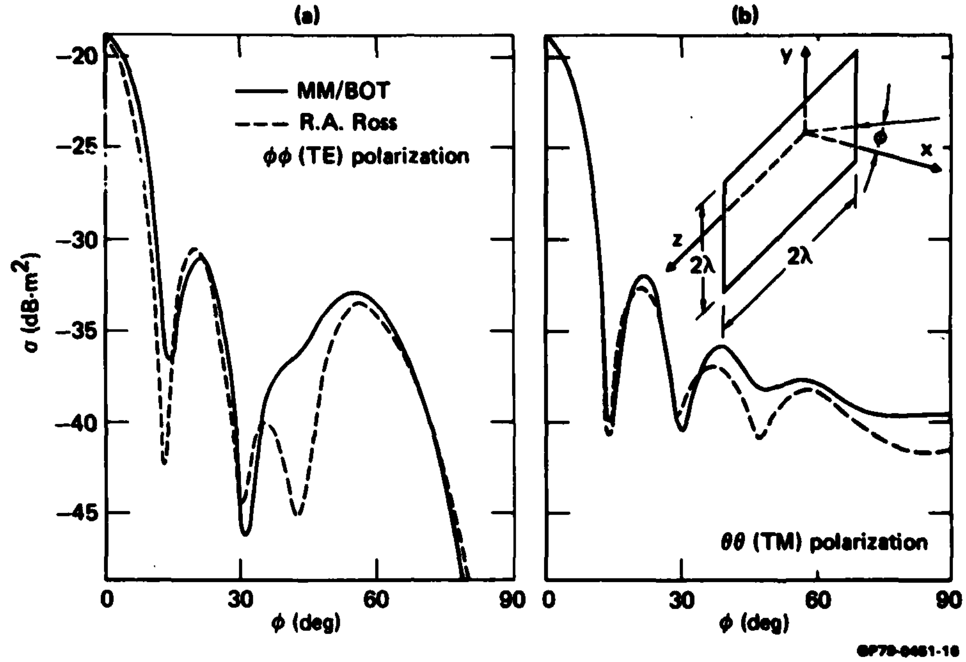

Figure 16. Monostatic scattering cross section for a square plate.

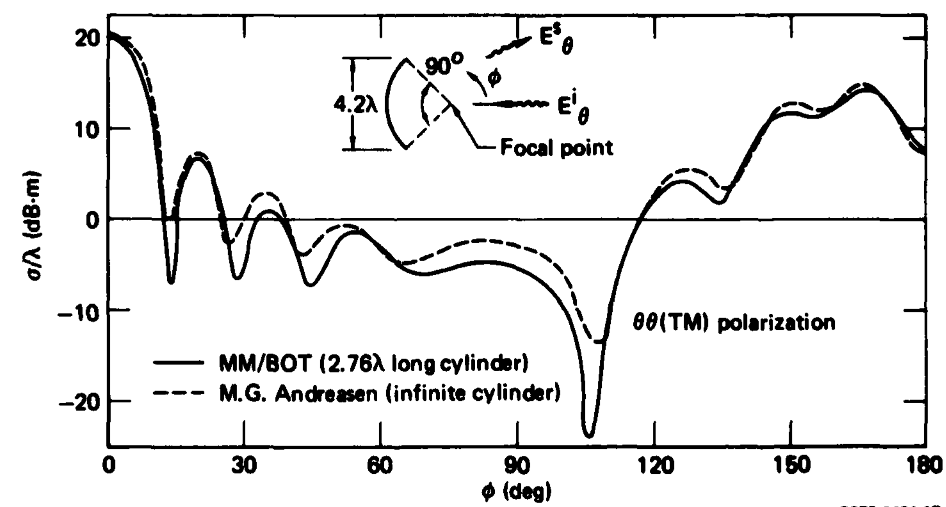

Figure 17. Bistatic scattering cross section for parabolic cylinder; broadside incidence ($\theta_i = 90^o$, $\phi_i = 0^o$).

8.2 Validation of Near Field and Aperture Analysis

Validation of the near-field formulation for the electric and magnetic fields is shown in the subsequent examples. In this phase of the investigation, the fields were computed by the MM/BOT technique for points at distances << λ from the radiating or scattering surfaces. As a benchmark, the exact boundary value solution for an infinite right-circular cylinder fed with a ϕ-polarized slit was used (Figure 18).[27] The slit subtended an angle of ϕ_o degrees and was excited with a uniform field. If the field is sampled near the cylinder, the predictions of the MM/BOT analysis for a finite cylinder can be compared with the exact (classical) solution obtained for

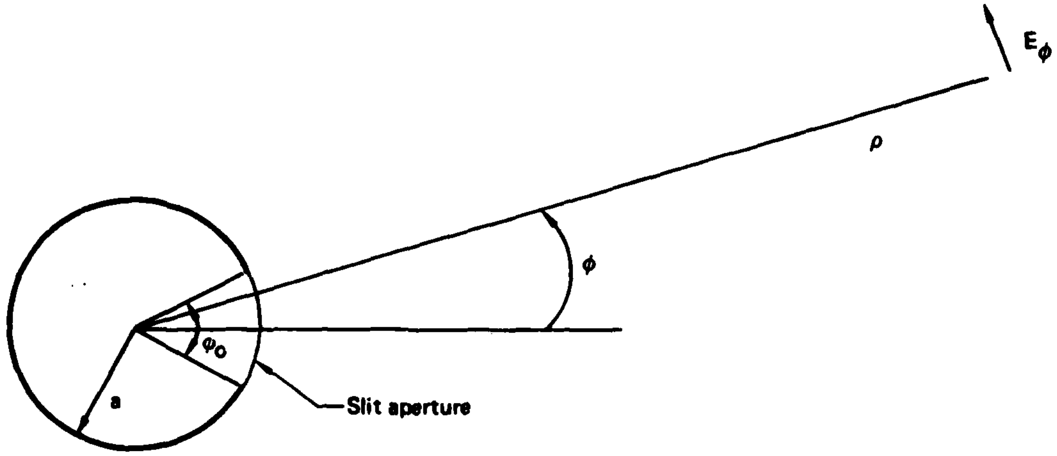

$$\text{Aperture field: } \begin{cases} E_o, & |\phi| < \phi_o \\ 0, & |\phi| > \phi_o \end{cases}$$

$$E_\phi = \frac{j\beta}{\omega\epsilon} \sum_{n=-\infty}^{\infty} b_n H_n^{(2)'}(\beta\rho) e^{jn\phi}, \quad \beta = \frac{2\pi}{\lambda}$$

$$H_z = \sum_{n=-\infty}^{\infty} b_n H_n^{(2)}(\beta\rho) e^{jn\phi}$$

$$E_\rho = \frac{1}{j\omega\rho\epsilon} \frac{\partial H_z}{\partial \phi} \quad \text{where } b_n = \frac{\omega\epsilon}{j\beta} \frac{E_o}{n\pi} \sin\frac{n\phi_o}{2} \frac{1}{H_n^{(2)'}(\beta a)}$$

GP79-0461-18

Figure 18. Classical solution for slit cylinder (ϕ - excited slit).

the infinite cylinder. A comparison of these solutions for a cylinder with ka = 1.35 and a slit of 45° is shown in Figure 19. For the MM/BOT analysis, the cylinder length was 2.76 λ long and the slit length was 2 λ. The near fields are sampled along a line bisecting the aperture, resulting in $E_\rho = 0$. The closest field sampling was at 1.2a which corresponds to 0.2a (= 0.04 λ) from the plane of the aperture. The calculations using four and seven modes produced practically the same results. Also shown in Figure 19 are the fields obtained from a patch near-field formulation in which the sampled fields are averaged over a flat strip. The large discrepancy of the patch results from the exact solution at points near the body is due to the fact that in this region the EM wave departs significantly from being planar. At distances ∿ 10 λ, the patch and point formulations coalesce. (As expected, at these distances, the classical solution for the infinite cylinder and the BOT results for the finite cylinder diverge.)

In Figure 20, the three near-field components sampled at a radial line at $\phi = 45°$ to the aperture center are given. Again, the results of the exact and the MM/BOT solutions are in excellent agreement. The corresponding results for field points sampled at $\phi = 90°$ are shown in Figure 21. At sampling distances >> λ from the BOT, E_ρ decreases and the EM wave front tends to approach being planar. Finally, the near fields for a slit subtending 22.5° are shown in Figure 22. In these calculations, 4 modes were used and 33 points defined the circumference of the cylinder. Again there was close agreement between the exact and MM/BOT solutions.

An application of the aperture-coupled field analysis of Section 7 is depicted in Figure 23. The internal fields, sampled along a radial line bisecting the aperture, are induced by a broadside TM illumination of a right circular cylinder. In the BOT calculations, the cylinder length was 5.52 λ, with the aperture subtending 22.5° and an axial length of 4.96 λ. Senior[28] considered the infinitely long cylinder with a 20° infinite slit and computed only the axial electric field, E_z. As can be seen, the BOT analysis is in good agreement with this result.

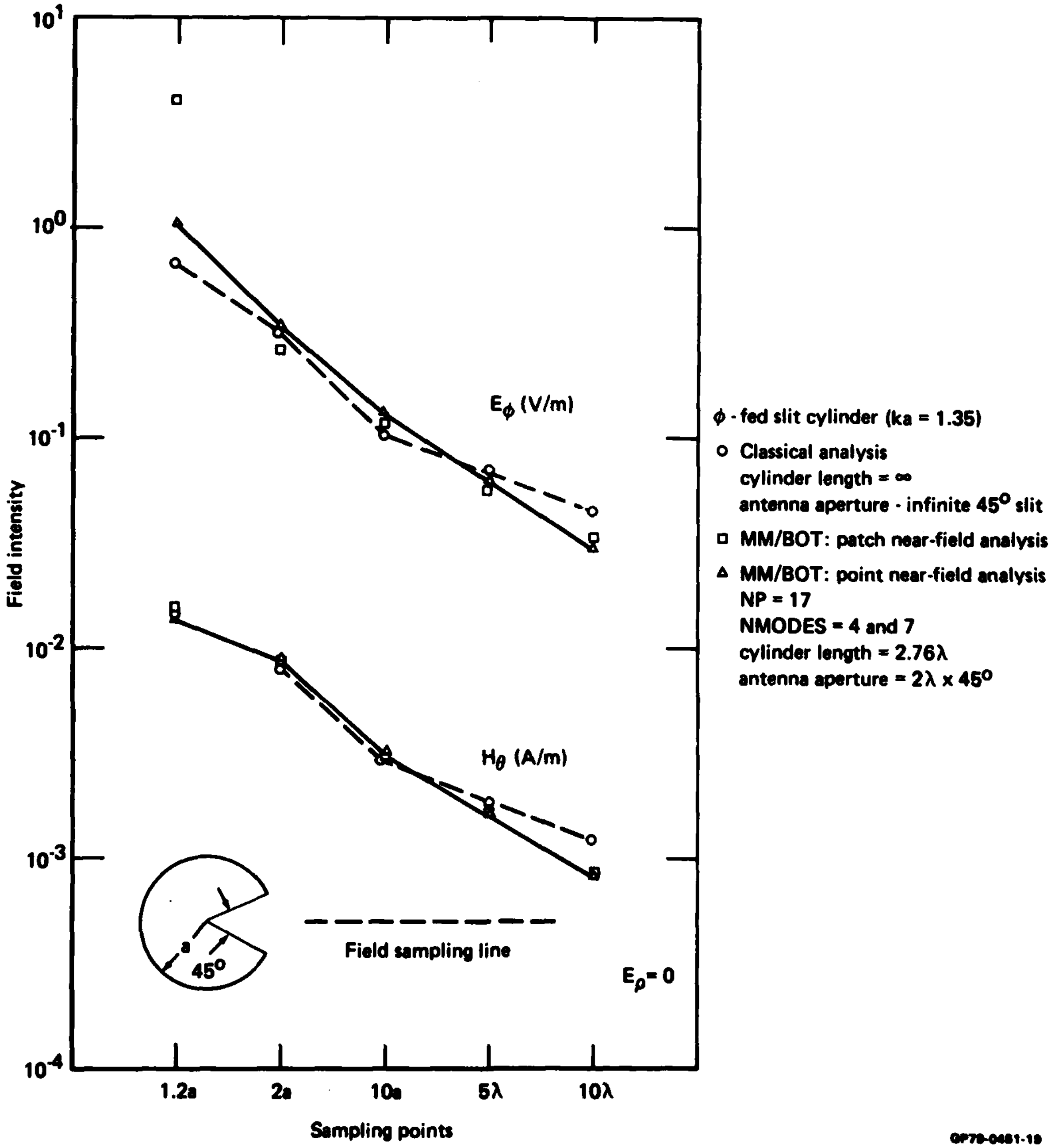

Figure 19. Computation of near fields for slit cylinder at $\phi = 0$ (slit angle = 45°)

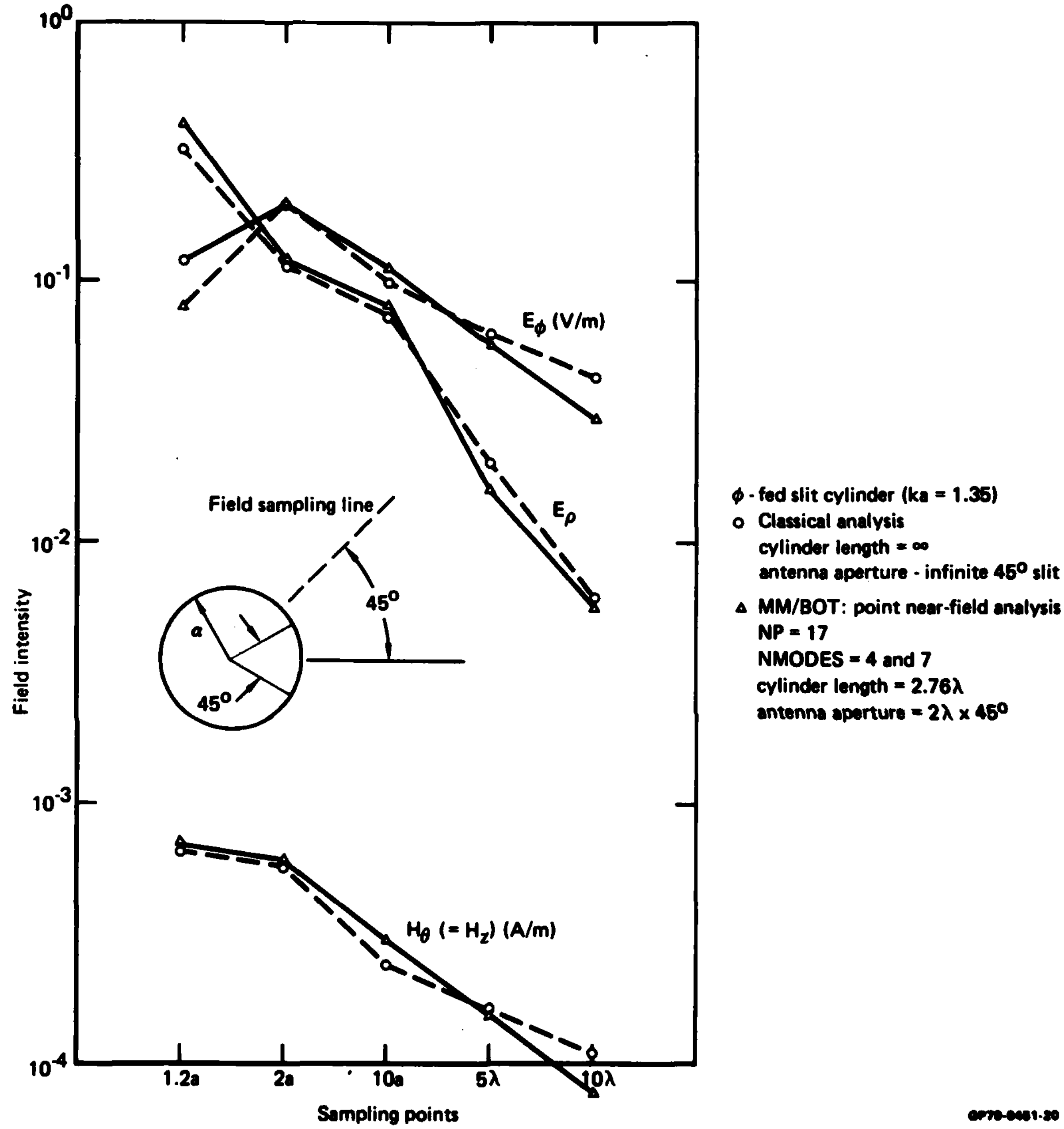

Figure 20. Computation of near fields for slit cylinder at ϕ = 45° (slit angle = 45°)

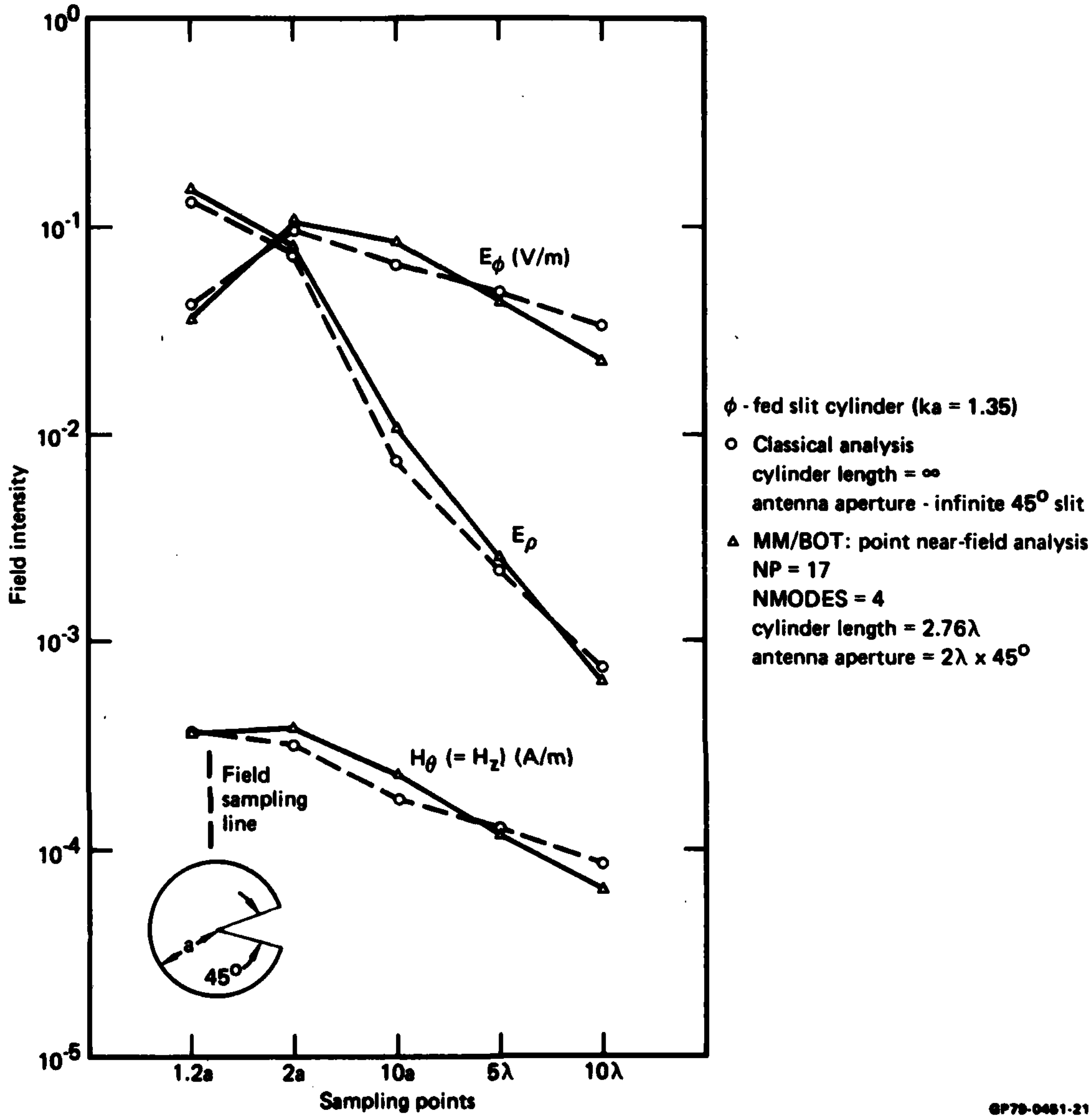

Figure 21. Computation of near fields for slit cylinder at ϕ = 90° (slit angle = 45°)

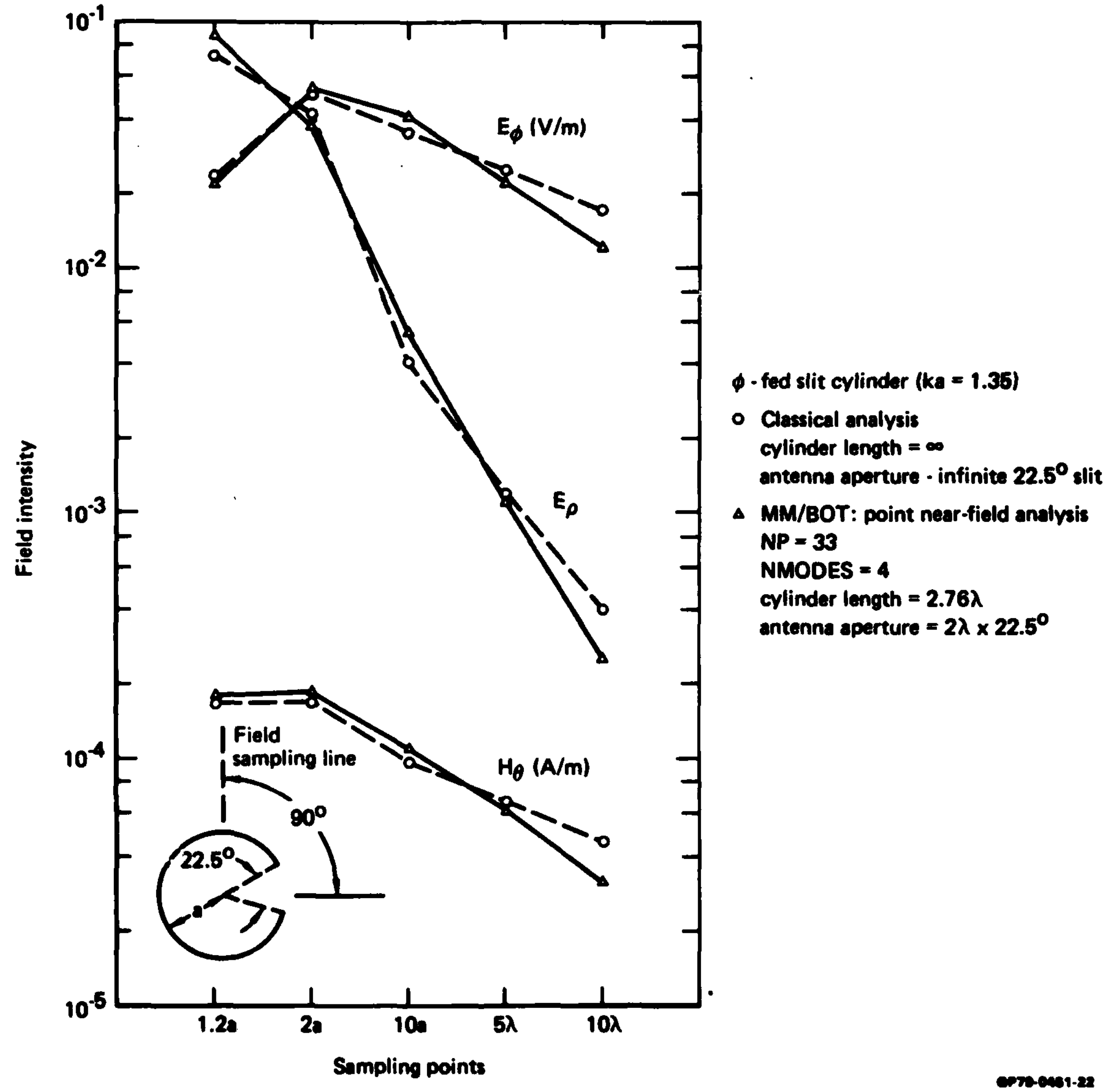

Figure 22. Computation of near fields for slit cylinder at $\phi = 90^{\circ}$ (slit angle = 22.5°)

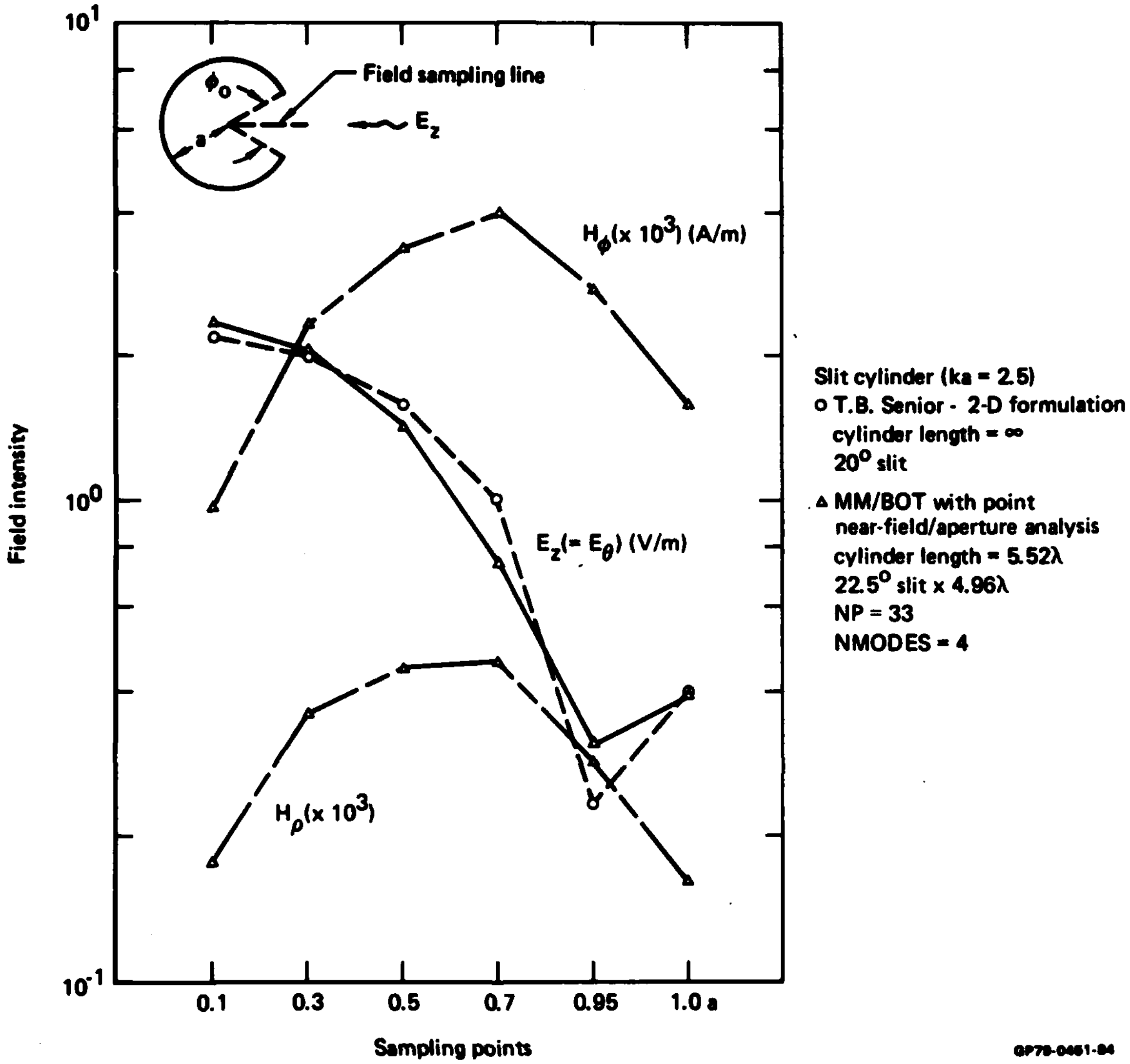

GP79-0461-84

Figure 23. Computation of aperture-coupled fields.

9. COMPUTER IMPLEMENTATION

The MM/BOT formulation described in the preceding sections was implemented with a computer algorithm which is described in detail in Volume II of this report. The overall structure of the program flow compares with that of the MM/BOR codes. The computational complexity is approximately equivalent for both MM/BOT and MM/BOR for a given size body. The matrix fill-times are comparable. The major differences lie in the fact that the modes in the present analysis do not decouple as in the MM/BOR, although, in general, the resulting network matrices remain diagonally strong and have certain symmetries [i.e., Equations (30-31)]. For sufficient accuracy, the off-diagonal submatrices for $m \neq n$ can sometimes be deleted from the computation without excessive error penalty (i.e., Figures 11-12).

Adequate computational accuracy is achieved when the BOT surface is segmented into strips $\gtrless 0.15\ \lambda$ in width. The number of axial modes chosen is dependent upon the spatial accuracy desired for the surface currents. While the examples shown in the validation section involved mostly right-circular cylinders, the present formalism is capable of treating any asymmetric BOT, such as a wing section. An example of this case is given in Volume II.

REFERENCES

1. R. Mittra (Editor), Computer Techniques for Electromagnetics (Pergamon Press, New York, 1973).
2. L. N. Medgyesi-Mitschang, A Method of Moments Formulation for Bodies of Translation, Proc. 1978 International Symposium on Antennas and Propagation (1978), pp. 112-115.
3. L. N. Medgyesi-Mitschang, Scattering from Thin Plates and Finite Curved Surfaces, Proc. 1979 International Symposium on Antennas and Propagation (1979), pp. 155-158.
4. J. R. Mautz and R. F. Harrington, Radiation and Scattering from Bodies of Revolution, Appl. Sci. Res. 20, 405 (1969).
5. R. F. Harrington, Matrix Methods for Field Problems, Proc. IEEE 55, 136 (1967).
6. M. G. Andreasen, Scattering from Parallel Metallic Cylinders with Arbitrary Cross Sections, IEEE Trans. Antennas Propagat. AP-12, 746 (1964).
7. R. F. Wallenberg and R. F. Harrington, Radiation from Apertures in Conducting Cylinders of Arbitrary Cross Sections, IEEE Trans. Antennas Propagat. AP-17, 56 (1969).
8. D. R. Wilton and R. Mittra, New Numerical Approach to the Calculation of EM Scattering Properties of Two-Dimensional Bodies of Arbitrary Cross Section, IEEE Trans. Antennas Propagat. AP-20, 310 (1972).
9. P. Ya. Ufimtsev, Diffraction of Plane Electromagnetic Waves by a Thin Cylindrical Conductor, Radioteck. Elekchtron. 7, 241 (1962).
10. R. B. Kieburtz, Scattering by a Finite Cylinder, in Electromagnetic Theory and Antennas, Part 1, E. C. Jordan, Ed. (Pergamon Press, New York, 1963) pp. 145-156.
11. A. T. Fialkovskii, Scattering of Plane Electromagnetic Waves by a Thin, Cylindrical Conductor of Finite Length, Soviet Phys.-Tech. Phys. 11, 1300-1304.
12. A. W. Adey, Scattering of Electromagnetic Waves by Long Cylinders, Electronic Radio Eng. 149 (1958).

13. W. E. Williams, Diffraction by a Cylinder of Finite Length, Proc. Cambridge Phil. Soc. 52, 322 (1956).
14. C. C. Kao, Three-Dimensional Electromagnetic Scattering from a Circular Tube of Finite Length, J. Appl. Phys. 40, 4732 (1969).
15. C. C. Kao, Electromagnetic Scattering from a Finite Tubular Cylinder: Numerical Solutions, Radio Sci. 5, 617 (1970).
16. W. A. Davis and R. Mittra, A New Approach to the Thin Scatterer Problem Using the Hybrid Equation, IEEE Proc. Antennas and Propagat. AP-25, 402 (1977).
17. R. M. Bevensee, The Syracuse Computer Code for Radiation and Scattering from Bodies of Revolution, Extended for Near-Field Computations, Lawrence Livermore Laboratory Report UCRL-51622 (May 1974).
18. H. A. Bethe, Theory of Diffraction by Small Holes, Phys. Rev. 66, 163 (1944).
19. C. J. Bouwkamp, Diffraction Theory Reports Prog. in Phys. 17, 75 (1954).
20. R. E. Collin, Field Theory for Guided Waves (McGraw-Hill, 1960) pp. 285-302.
21. C. T. Johnk et al., Electromagnetic Penetration into Cylindrical Enclosures, Sci. Report No. 17, University of Colorado, Boulder, prepared under Contract No. N00173-74-C-0556, January 1976.
22. H. K. Schuman, Coupling Through Rotationally Symmetric Apertures in Cavities of Revolution, RADC-TR-77-214, June 1977, A042093.
23. H. K. Schuman and D. E. Warren, Aperture Coupling in Bodies of Revolution, IEEE Trans. Antennas Propagat. AP-26, 778 (1978).
24. H. K. Schuman, Circumferential Distribution of Scattering Current and Small Hole Coupling for Thin Finite Cylinders, IEEE Proc. Antennas Propagat. AP-27, 103 (1979).
25. S. A. Schelkunoff, Field Equivalence Theorems, Commun. Pure Appl. Math. 4, 43 (1951).
26. R. A. Ross, Radar Cross Section of Rectangular Flat Plates as a Function of Aspect Angle, IEEE Trans. Antennas Propagat. AP-14, 329 (1966).
27. E. C. Jordan, Electromagnetic Waves and Radiating Systems (Prentice-Hall, Inc., 1950).
28. T. B. A. Senior, Electromagnetic Field Penetration into a Cylindrical Cavity, IEEE Trans. Electromagn. Compat. EMC-18, 71 (1976).

g